Fall 2006

Numerical analysis of the operation of a water cannon

Teymuraz G. Bitadze
New Jersey Institute of Technology

ABSTRACT

NUMERICAL ANALYSIS OF THE OPERATION OF A WATER CANNON

by
Teymuraz G. Bitadze

This study was designed to investigate the operational process of a launcher for generation of high speed water projectiles, and it involved the optimization of the geometry of a launcher body. The objective of the optimization of the internal geometry was to increase the effective momentum of the projectile while the optimization of the external geometry resulted in the reduction of the mass of the launcher.

In the course of the optimization of the internal geometry the exit velocity variation was determined, and used to compute an effective projectile momentum, which actually affects a workpiece. In this research, it was assumed that the effective momentum is generated if the velocity of the impacting fluid exceeds the critical velocity. A cutoff factor was introduced in order to separate a part of projectile which generates an effective momentum. A numerical model of the process developed by G. Atanov was used to determine the exit water velocity while a C++ program was developed in order to determine the effective momentum of the projectile at various launcher geometries. The optimization involved the approximation of the internal launcher geometry by a combination of a cylinder (barrel) and two cones (nozzle), the length and diameters of which constituted the process. The near optimal values of these variables were determined and have shown that the optimization of the nozzle geometry enables an increase in the effective momentum of a projectile by 40%.

The second problem surveyed the effect of the variation of the external geometry of the water cannon on its weight. An array of the cannon geometries, which assured the

sufficient strength of the construction, was investigated and a shape minimizing the mass of the device was found. The Atanov model was used to determine the pressure distribution within the water cannon, and the computation package Pro-MECHANICA was applied to determine the stresses in the cannon body. The external geometry was selected so that at each cross section the actual stresses, static, and dynamic did not exceed the critical stresses determined by the use of the von Mises criterion. The analysis was carried out at the external geometry of the existing cannon prototype and had shown that the geometry optimization enables a reduction of the cannon mass by 15 %.

The third part of the experiment was devoted to investigate water slug-target interaction. It was carried out through an assimilation of a demining and a concrete demolition processes with a high-speed water projectile. The experiment has shown the importance of stand-off distance with different types of targets.

NUMERICAL ANALYSIS OF THE OPERATION OF A WATER CANNON

by
Teymuraz G. Bitadze

A Thesis
Submitted to the Faculty of
New Jersey Institute of Technology
in Partial Fulfillment of the Requirements for the Degree of
Master of Science in Mechanical Engineering

Department of Mechanical Engineering

January 2007

Blank Page

APPROVAL PAGE

NUMERICAL ANALYSIS OF THE OPERATION OF A WATER CANNON

Teymuraz G. Bitadze

Dr. Ernest S Geskin, Thesis Advisor | Date
Professor of Mechanical Engineering, NJIT

Dr. Rajpal S. Sodhi, Committee Member | Date
Professor of Mechanical Engineering, NJIT

Dr. Chao Zhu, Committee Member | Date
Associate Professor of Mechanical Engineering, NJIT

BIOGRAPHICAL SKETCH

Author: Teymuraz G. Bitadze

Degree: Master of Science

Date: January 2007

Undergraduate and Graduate Education:

- Master of Science in Mechanical Engineering
  New Jersey Institute of Technology, Newark, NJ, 2007

- Master /Bachelor of Science in Mechanical Engineering
  Moscow State Technical University, Russia, 2002

Major: Mechanical Engineering

This thesis is dedicated to Ernest S. Geskin

ACKNOWLEDGMENT

The author wishes to express his sincere gratitude to his advisor, Professor Ernest S. Geskin for his guidance, help, and constant encouragement throughout this research.

The author is grateful to Dr. Rajpal S. Sodhi and Dr. Chao Zhu for serving as members of the committee.

Special thanks to Oleg Petrenko for his valuable suggestions.

TABLE OF CONTENTS

LIST OF TABLES

LIST OF FIGURES

NOMENCLATURE

NL_{con}	length of the conic part of the nozzle
M_o	water load mass
L_{bar}	barrel length
D_n2	nozzle outlet diameter
D_n1	nozzle inlet diameter
r_{col}	collimator radius
t_{sto}	time of integration (3.1) stop
ρ_o	water density at normal conditions
v	outflow velocity
v_{max}	maximum outflow velocity attained during a shot
L_{nzl}	length of the nozzle
R_{inlet}	inlet radius of the nozzle
R_{outlet}	outlet radius of the nozzle
R_{con1}	radius of the connection between two cones constituting the nozzle
L_{con1}	length of the first of the two cones constituting the nozzle
y	optimization variable, $y=R_{con1}$
x	optimization variable, $x=L_{con1}$
D	dimensionless number
V	water velocity
σ	yield stress
$\sigma_1, \sigma_2, \sigma_3$	principal stresses

σ_{eq} von Mises stress

ρ water density

CHAPTER 1

INTRODUCTION

There is a wide range of applications of super high-speed water projectiles generated by water cannons. They can be used for material processing, explosive neutralization, structure demolition, and as specific surgical tools in medicine, and other applications. Waterjet technology is used in many other processes, such as cleaning, shaping, cutting, machining, drilling, and polishing. A numerical analysis of the existing water cannon prototype and experimental results helped to develop the technique of system optimization. Another technique, developed by G.A. Atanov, based on the study of the material and momentum conservation equations was used for analysis of water acceleration. In present work, device improvement by investigating numerical methods for the water cannon optimization was demonstrated.

CHAPTER 2

MISSION STATEMENT [4]

The objective of this work is to evaluate quasi-optimal values of the operational and design parameters of a water cannon for generation of high speed water projectiles (impulsive jets). The water cannon is a device where energy is used to propel a liquid (water load) placed in a barrel with an attached nozzle. In a way, the water cannon is a rifle a liquid bullet. The modification of a converging nozzle attached to the barrel of the cannon enables to increase the speed of the generated projectile by two or three times and perhaps more. The actual potential of the water cannon is yet to be determined.

The additional acceleration of the water projectile is due to the flow converging in the nozzle and superposition of the compression and rarefaction waves in the fluid. However, the main contribution to the generation of high velocity projectiles is the energy redistribution in the course of the unsteady flow in the barrel and nozzle. As a result of this redistribution, the front of the water load accelerates to a high velocity. It is obvious that the complicated chain of energy transfer processes (from an energy source to the liquid load and then within the liquid projectile) is highly parameter sensitive. Existing water cannons were designed on the bases of feasibility consideration only. A number of the performed experiments, both industrial and laboratory, evidently demonstrate process feasibility [1]. Numerical models describing velocity and pressure within the cannon were also developed and validated [2]. It is necessary now to utilize the acquired knowledge for evaluation both of cannon design and operation. Such evaluation will enable researchers to improve this device as well as to develop techniques for development of other jet-based devices and processes.

Two optimization problems were addressed in this study. The first problem involved selection of the interior geometry of the cannon as well as the specific energy supply which maximizes the effective (available) momentum of the projectile. In this problem the objective function is the effective momentum of the projectile while the specific energy and cannon interior geometry are independent variables. Two numerical techniques were used to evaluate the sought variables. The first one involved a numerical evaluation of various combinations of the control variables and a comparison of the obtained value of the objective function. A factorial analysis was used in this study.

The second problem involved reduction of the cannon weight at a given pressure distribution along the cannon. Commercial packages were used for determination of the stress distribution in axysymmetric enclosures at a given pressure distribution along the cannon axis and the cannon geometry. Then the yield criterion was evaluated for three different geometries. The comparison between the actual maximal value of this criterion and its critical value was used to evaluate the cannon design. The performed computations suggested improvements of the water cannon design and operation.

CHAPTER 3

EVALUATION OF THE CANNON GEOMETRY

3.1 Problem Overview

The water cannon design is illustrated by the schematics in Figures 3.1 and 3.2, where powder combustion is used as an energy source.

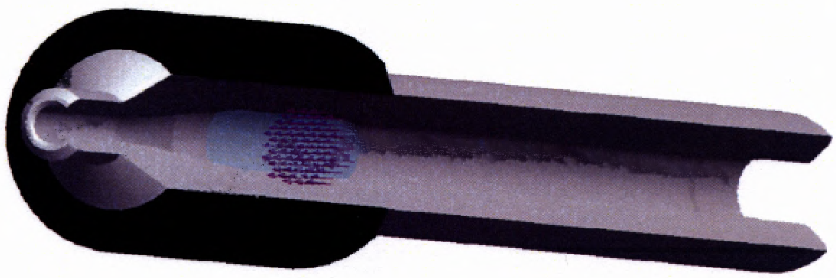

Figure 3.1 General schematic of the cannon.

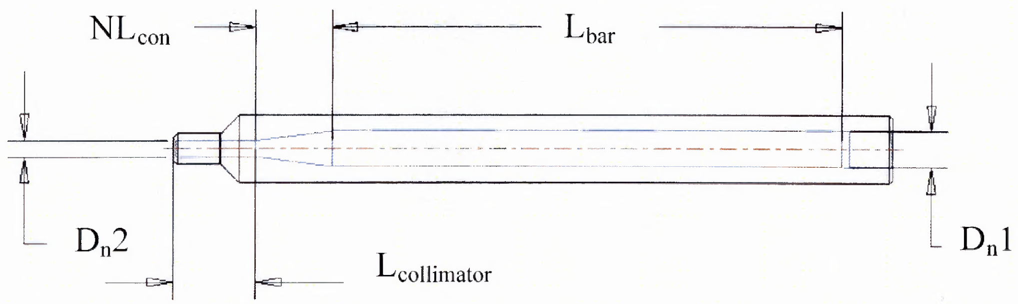

Figure 3.2 Detailed view of the barrel.

A computational procedure for prediction of the pressure and velocity distribution along the water cannon, developed earlier [2], constitutes a base for evaluation of the device efficiency. The examples of the application of this procedure are depicted on

Figure 3.3 which shows velocity distribution during the process. The results are obtained for the different length of the barrel. The objective of the cannon operation is formation of the projectiles which bring about deformation of ductile and breakage of the brittle materials. The effect of an impacting particle on a target is determined by the dimensionless damage number (D)

$$D=\rho V^2/\sigma \tag{3.1}$$

If the actual damage number is less than the critical one, the impact does not affect the target. Total effect of the projectile can be evaluated by the momentum of water and its velocity, which assures the magnitude of the damage number exceeds the critical level. Because the maximum velocity of the water is attained at the beginning of the process, and the velocity function is monotonous, the water momentum which affects the target (the effective water momentum) is given by the equation below.

$$M_{effective} = \int_{t}^{t_{cutoff}} \rho F \upsilon^2 dt \tag{3.2}$$

Here t_{cutoff} determines the time when the velocity of the jet drops below the critical level. As it follows from (Figure 3.3) the monotonous change of the water exit velocity enables to relate the water velocity to the time.

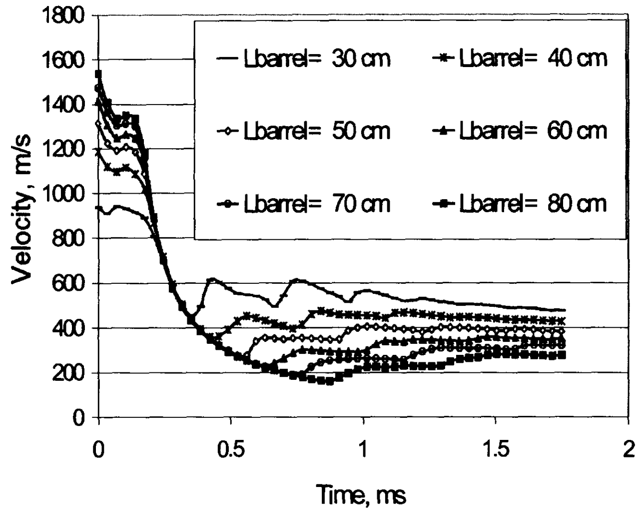

Figure 3.3 Outflow velocity vs. time at different barrel length.

The integral (3.2) can be used for evaluation of the effective momentum. In order to achieve this it is necessary to determine the t_{cutoff}. In principle this time is determined by the process duration when the water velocity reaches the critical level determined by the minimal value of the damage number. However, because the value of D for a given target is usually unknown, it is better to determine the t_{cutoff} by the time when the exit velocity constitutes a selected fraction of the maximal water velocity. From a practical consideration, in this analysis the cutoff velocity constitutes 85% of the total velocity.

Determination of operational and design variables can be reduced to the selection of the values of the variables which maximize the integral (3.2) while the process constraints are determined by the system of equations of relating fields of the water pressure and velocity. The direct search of the quasi-optimal values of the process variable (Factorial Analysis) is used for solving a problem in question. A large number of process variable and complicated process models made it difficult if not impossible to use more sophisticated optimization techniques.

Variation of the water velocity and pressure along the cannon axis in the course of the projectile formation is depicted on Figures 3.4 and 3.5.

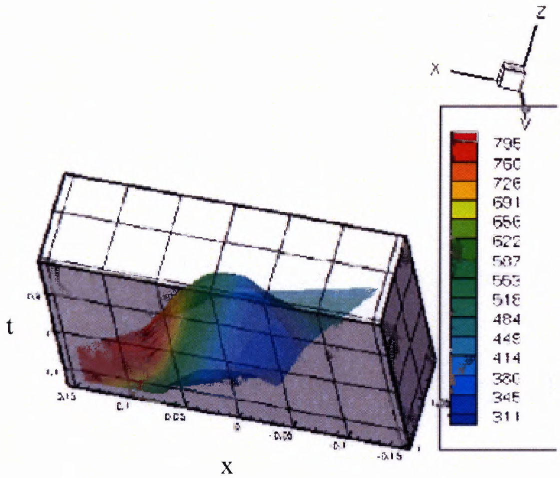

Figure 3.4 Water velocity distribution plot with 100g water load.

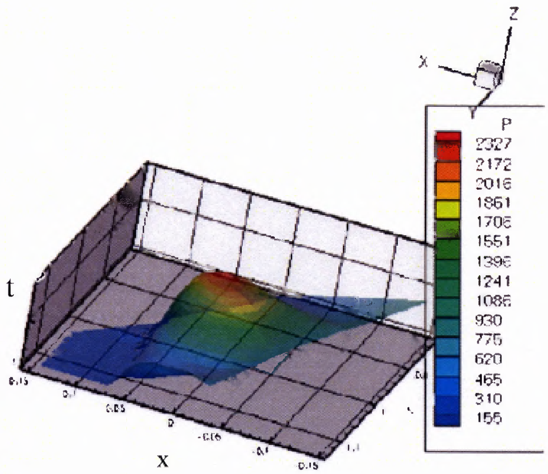

Figure 3.5 Pressure distribution plot with 100g water load.

These figures show respectively velocity and pressure in x-t space, where x represents the length of the nozzle, and t - the moment of inflow. The entire set of figures which represent the water velocity and pressure along the cannon axis is illustrated in the Appendix A.

CHAPTER 4

FACTORIAL ANALYSIS

The objective of the performed search was to determine the profile of the water cannon and the specific energy of the process. The specific energy is determined by the ratio between the water and powder mass, while the geometry of the cannon interior is characterized by the length of the conic part of the nozzle, nozzle inlet diameter, nozzle outlet diameter, collimator length, and the barrel length. A preliminary qualitative analysis and quantitative estimation were used to determine the range of the process variables, and then the selected process variables were digitized, and various combinations of these variables were randomly selected (Table 4.1).

Table 4.1 Sets of Varied Variables

Set 1			**Set 2**			**Set 3**		
L_{bar}	D_{n2}	D_{n1}	L_{bar}	D_{n2}	D_{n1}	L_{bar}	D_{n2}	D_{n1}
280e-3	5e-3	30e-3	290e-3	19e-3	31e-3	270e-3	21e-3	29.5e-3
380e-3	15e-3	32e-3	300e-3	18e-3	32e-3	260e-3	22e-3	29e-3
700e-3	20e-3	64e-3	310e-3	17e-3	33e-3	250e-3	23e-3	28.5e-3

For the research purposes three sets of parameters, which constitute F of the integral (3.2), were used. Set 1 consists of 27 combinations, where the maximum and minimum impulse integral values are found, and the shaded cells represent actual parameters of the existing water cannon prototype. Set 2 contains parameters for greater length of the barrel (L_{bar}), smaller diameter of the nozzle (D_n2), and greater internal diameter of the barrel (D_n1), and Set 3 contains parameters for smaller L_{bar}, greater D_n2, and smaller D_n1. Total of 81 possible combinations of varied parameters and their various modes of the process output at non-monotonous function behavior were examined, 27 of which are depicted by graphs in Appendix B.

Exploring various possibilities of the geometric parameters allows understanding crucial factors influencing the momentum. This quantitative analysis determines the optimal dimensions to create "the most powerful" water projectile. Evaluation of the changes occurring throughout the barrel and the nozzle, due to a change of each parameter determines a set of boundaries which provides the upper limit of the functions affecting the process. It should be noted that the best of the observed results have been obtained at the existing operational and design condition, which have been found in the course of the experimental trial and error research. A peculiar momentum change is depicted on Figure 4.1, where the maximum effective momentum is reached at a shorter NL_{con} and with the highest water load. For the illustration the graph with the minimal value of the integral (3.2) in the same domain of Set 1 is presented on Figure 4.2.

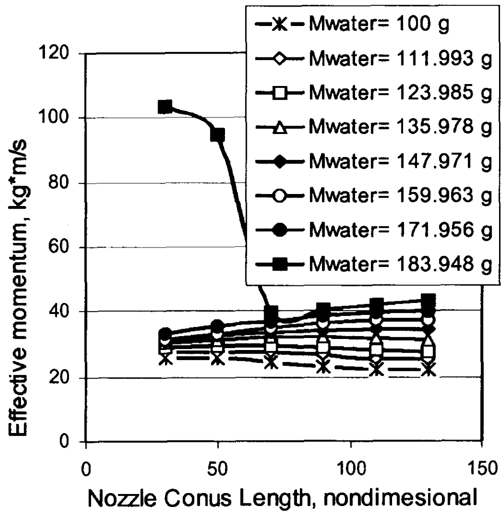

Figure 4.1 Impulse integral vs. water load - 1.

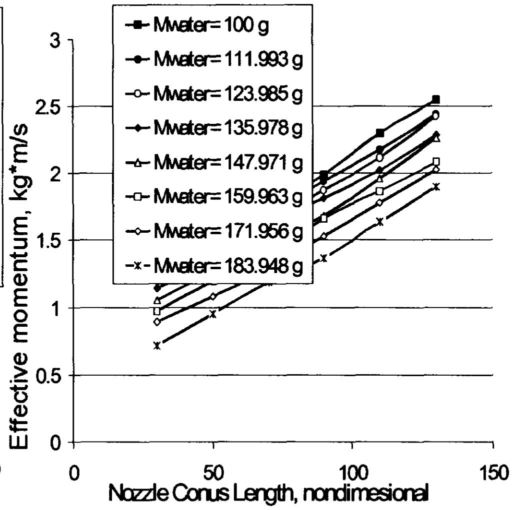

Figure 4.2 Impulse integral vs. water load - 2.

The effect of the cutoff factor on the cannon performance is illustrated by Figures 4.3 and 4.4. The Figure 4.3 shows two cases (not optimal) of the exit velocity variation determined by the nozzle length. The variation of the effective jet momentum in the processes depicted on Figure 4.3 is shown on Figure 4.4. As it follows from these two figures, practically insignificant velocity difference (7%) brings about dramatic difference in the process effectiveness (almost 100%). This result is due to the velocity cutoff, which determines the duration of the interval when the effective jet is generated. Due to the cutoff velocity, a small difference in the flow velocity results in significant difference in the duration of the formation of the effective water stream. In fact, such difference in the estimation of the process effectiveness reflects its actual performance. If the impulse of the projectile less than critical one, regardless of the magnitude of this difference the projectile does not affect the target. The Figures 4.3 and 4.4 evidently demonstrate the strong effect of the operational and design conditions of the process results.

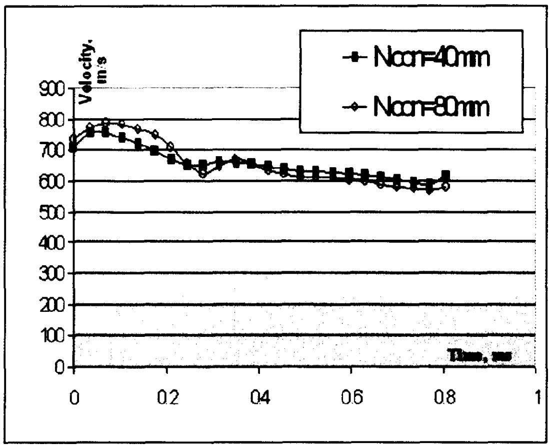

Figure 4.3 Outflow velocity.

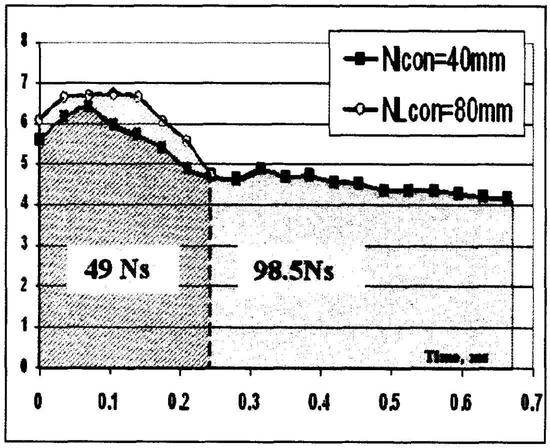

Figure 4.4 Momentum integral at cutoff=0.8.

CHAPTER 5

WEIGHT MINIMIZATION

Previously, the emphasis was given to the improvement of the water flow through the water cannon. Another optimization objective is the reduction of the cannon weight. The cannon should withstand the maximal stresses developed in the course of the projectile over the entire cannon volume but not to exceed the critical stresses determined by the von Mises criterion. The cannon design should minimize the thickness of the cannon wall, which assures a permissible level of the maximal stresses. The Pro-MECHANICA package was used to determine the stresses in the cannon wall at a point when pressure on it reaches its maximum value for the moment of time at 1.15 ms (Figure 5.1).

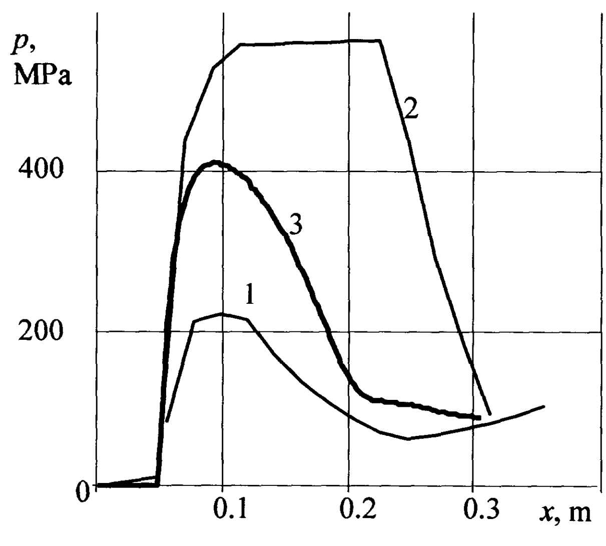

Figure 5.1 Water pressure distributions in a barrel for 1) 1.05 ms 2) 1.15 ms 3) 1.25 ms.

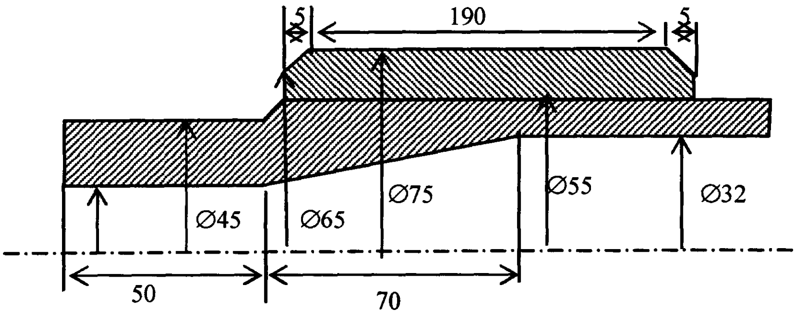

Figure 5.2 Water cannon sectional view.

The water pressure distribution in the barrel was obtained using the C++ code developed by O. Petrenko [3]. The detailed description of the water projectile formation is given in the next chapter.

Solving the optimization problem involves the Pro-MECHANICA analysis utilization, which allows carrying out of a stress analysis of the system with various physical and geometrical nonlinearities. The problem was solved in domain of the theory of elasticity with the consideration of contact deformations, and due to the symmetry the axysymmetric model was used to find the solution. Finite Element Model consists of 19,000 nodes, and the size of the element is 10e-3 m^2. A discretization is performed with the solid 8-node element which permits to solve the axysymmetric problems and build a fine mesh. The computations were carried out at the following steel properties: Young's modulus E = 2e+11 Pa, Poisson's ratio ν=0.3, friction coefficient between the barrel and the rim μ=0.2. Internal pressure calculated by Godunov method [4] is set up by mesh function in 128 dotes not connected to the nodes of the mesh using user defined function, which classifies data which needs to be read from the output file to the database. Pro-MECHANICA uses a linear interpolation for the load definition in nodes of the mesh.

According to the fourth energy method in strength theory:

$$\sigma_{eq} = \sqrt{1/2((\sigma_1 - \sigma_2)^2 + (\sigma_1 - \sigma_3)^2 + (\sigma_3 - \sigma_2))} \leq [\sigma] \qquad (5.1)$$

Where σ_{eq} - von Mises stress; $\sigma_1, \sigma_2, \sigma_3$ - principal stresses;

For the material of the actual device $[\sigma]$ = 1520 Mpa, von Mises stresses distribution plot is shown in the Figure 5.3.

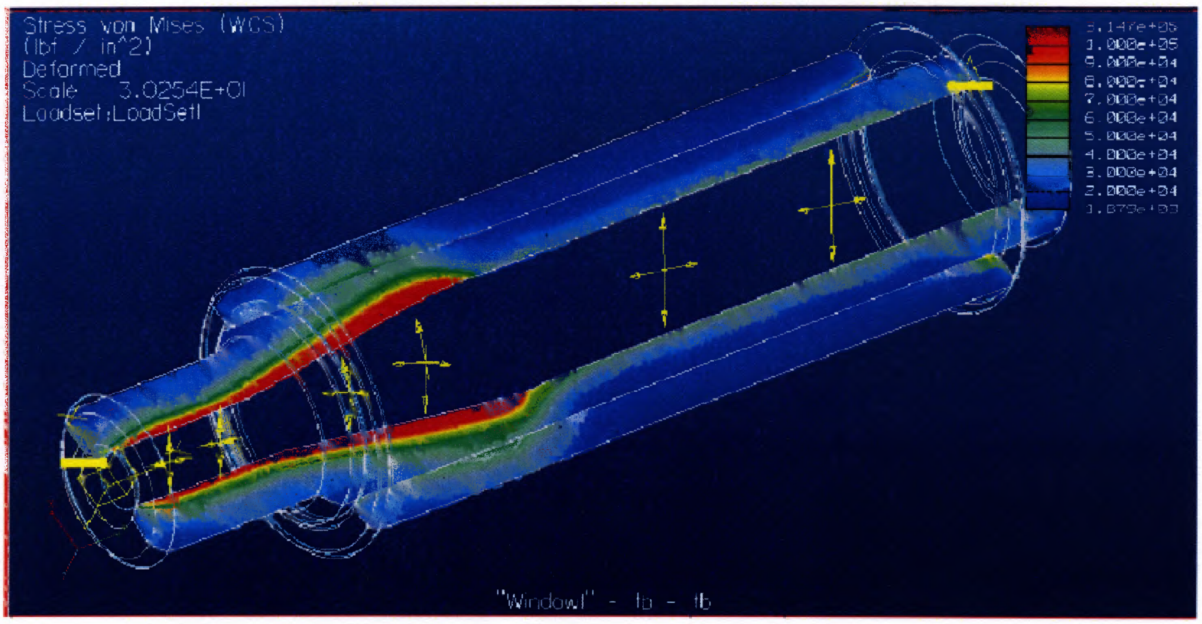

Figure 5.3 Von Mises stresses distribution plot.

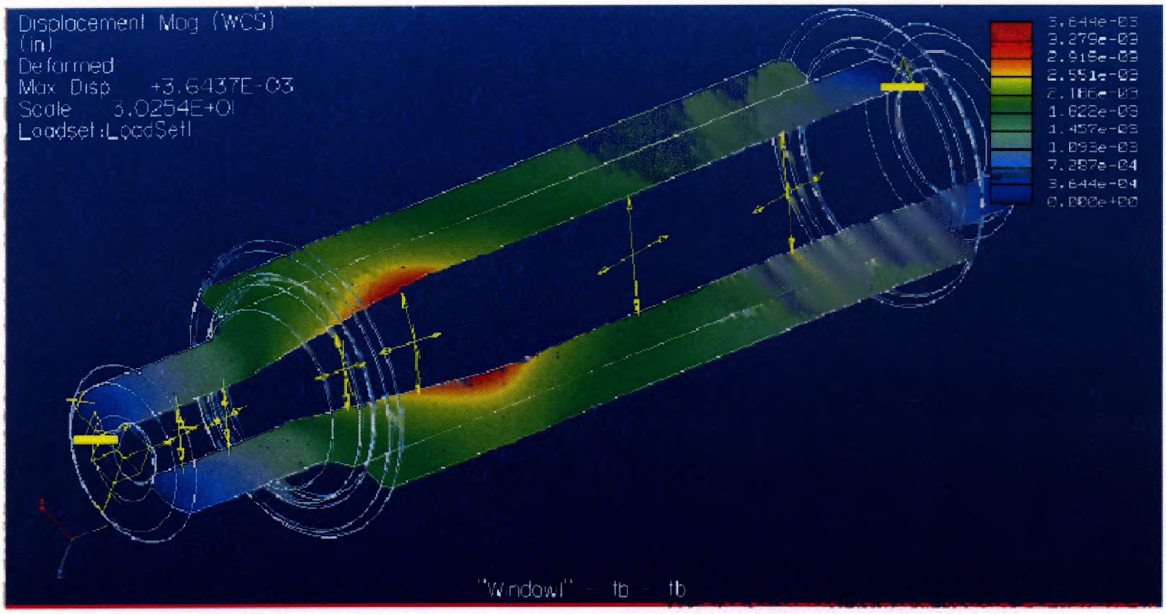

Figure 5.4 Displacement distribution plot.

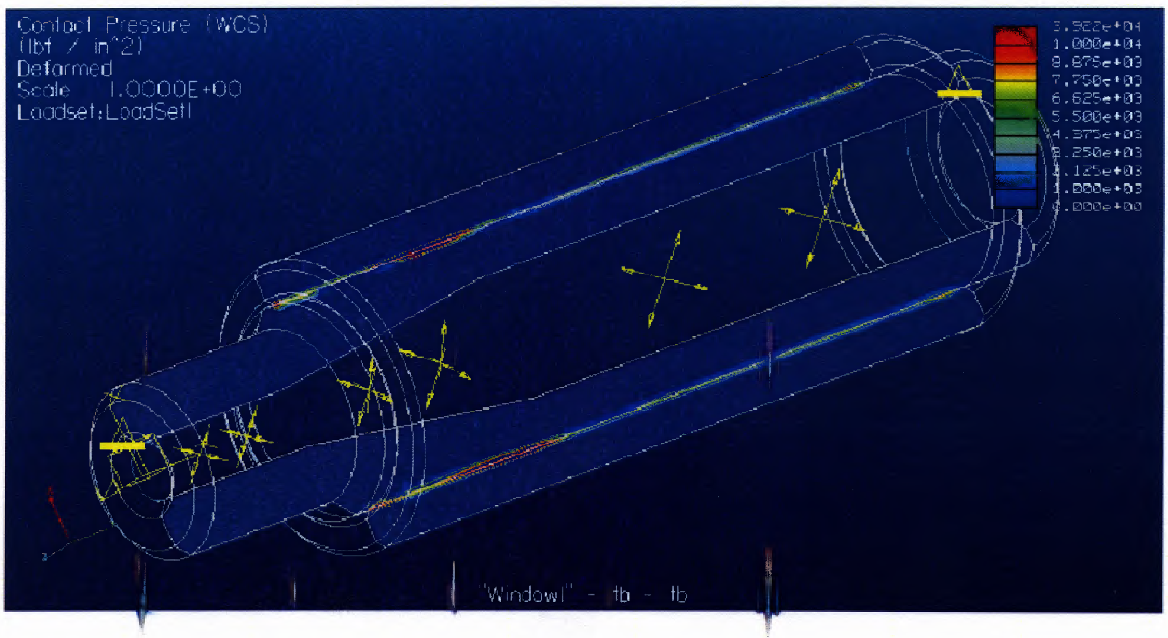

Figure 5.5 Contact pressure distribution plot.

It is expected that the weight of powder fed device will be in the range of 10-20 kg. The analyzing von Mises stresses distribution plot shown on Figure 5.3 it can be concluded that the design optimization enables us to reduce the cannon weight by 20-30% (the highest stress equals to 3.147e+05 lbf/in^2 = 2170Mpa comparatively to $[\sigma]$ = 1520 (Mpa).

Further reduction, perhaps by 50% can be achieved by the use of composite materials.

CHAPTER 6

PROJECTILE FORMATION MODELING [3]

The following description of the projectile formation is given to get some background of the process of water flow within the cannon. The water flow is defined by Navier-Stokes equations and the water constitutive equation. However this system of equations is very complicated to be solved in the general problem definition. Process peculiarities should be taken into account in order to simplify the equations to make solution practical.

The studied experimental water cannon and similar devices described in the introduction have the following range of parameters.

- Outflow water velocity: 700 – 2000 m/s
- Average water velocity in the barrel: 200 – 500 m/s
- Nozzle exit diameter: 10 – 20mm
- Water pressure: up to 1,000 MPa
- Angle of nozzle convergence: 7 – 10 degrees

These parameters define the assumptions that can be used to reduce the general system of equations. Small angle of the nozzle convergence allows reducing the problem to 1-D case. High velocities and relatively large characteristic dimensions yield high Reynolds number:

$$\mathrm{Re} = \frac{VD}{\nu} = 1000\mathrm{m/s} * 10^{-3}\mathrm{m}/10^{-6}\mathrm{s/m}^2 = 10^6 \tag{6.1}$$

Thus, it can be assumed that the flow is inviscid. At the high pressures attained in the cannon, water cannot be considered to be an incompressible fluid any more. Pressure of

1,000MPa results in 30% water volume reduction. The short time duration and the absence of strong shock waves make it possible to assume that the flow is isentropic.

The stated above assumptions were made by Dr. Atanov and resulted in the following system of equations:

$$\frac{\partial u}{\partial t}+u\frac{\partial u}{\partial x}=-\frac{1}{\rho}\frac{\partial P}{\partial x} \tag{6.2}$$

$$\frac{\partial \rho}{\partial t}+\rho\frac{\partial u}{\partial x}+u\left(\frac{\partial \rho}{\partial x}+\rho\frac{1}{F}\frac{\partial F}{\partial x}\right)=0 \tag{6.3}$$

$$\frac{P+B}{\rho^{n}}=const \tag{6.4}$$

These are 1-D dynamic equations of the momentum, mass balances, and the isentropic state. Boundary conditions for the above equations are defined from the principle of operation of the studied experimental water cannon. Initial velocities and pressure in the barrel are assumed to be zero. The pressure at the gas-liquid interface in the course of the process is equal to the pressure of the combustion product, while the pressure at free surface separating the liquid and the atmosphere is assumed to be zero. In the performed computations the entrance of the nozzle is taken to be the origin of the space coordinate x. The time origin is the moment of the combustion start. Therefore, the initial and the boundary conditions of this system of equations are as follows:

$$u\,(x,\,0)=0,\ \rho(x,\,0)=\rho_0,\ P(x,\,0)=0,\ P(-L_{brl},\,0)=Pg,\ x\in(-L_{brl}\,;\,-L_{brl}+L), \tag{6.5}$$

Using the isentropic equation (6.4) the number of the variables in the first two equations can be reduced from three parts to two and the system (6.2, 6.3, 6.4) can be reduced to the form of:

$$\frac{\partial u}{\partial t}+\frac{\partial}{\partial x}\left(\frac{u^2}{2}+\frac{\rho^{n-1}}{n-1}\right)=0 \tag{6.6}$$

$$\frac{\partial u}{\partial t}\rho F+\frac{\partial}{\partial x}uF=0 \tag{6.7}$$

The equations (6.6, 6.7) are written in non-dimensional form, the sound speed and density of water at normal conditions and barrel length were used for scaling. Integration of the system (6.6, 6.7) over an arbitrary domain in the x-t space yields:

$$\iint\left[\frac{\partial u}{\partial t}+\frac{\partial}{\partial x}\left(\frac{u^2}{2}+\frac{\rho^{n-1}}{n-1}\right)\right]dxdt=0 \tag{6.8}$$

$$\iint\left[\frac{\partial u}{\partial t}\rho F+\frac{\partial}{\partial x}uF\right]dxdt=0 \tag{6.9}$$

Using the Green formula we can rewrite system (6.8, 6.9) in the form of:

$$\oint\left[udx-\left(\frac{u^2}{2}+\frac{\rho^{n-1}}{n-1}\right)dt\right]=0 \tag{6.10}$$

$$\oint\left[\rho Fdx-u\rho Fdt\right]=0 \tag{6.11}$$

The computational procedure involved numerical solution of the system (6.10, 6.11). The technique is based on the finite difference method while the method of characteristics is used to relate fluid properties at the t and $t+\Delta t$ intervals. This method was suggested by Godunov (Godunov, 1976) and thus carries his name. The 1-D time-space computational domain was approximated by a trapezoidal grid with a constant number of x-steps equal at each time instance (Figure 6.1).

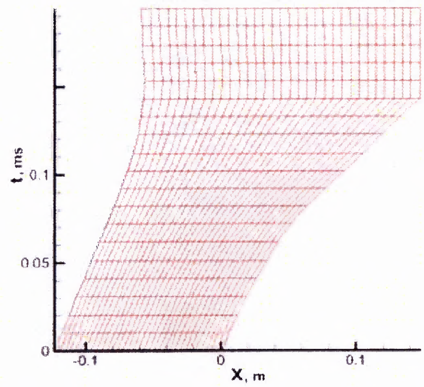

Figure 6.1 Schematic of the mesh.

The example of a grid cell is shown on Figure 6.2. Here the horizontal lines represent the

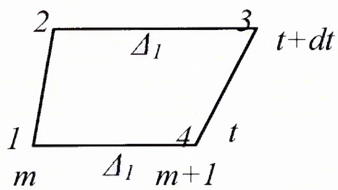

Figure 6.2 A grid cell schematic.

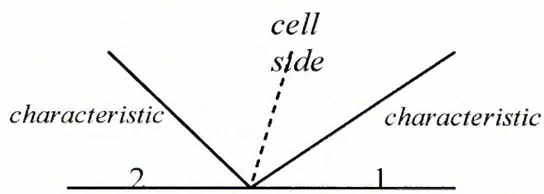

Figure 6.3 Schematic for equation (6.12), (6.13).

state of water at time instances t and $t+dt$. As the projectile moves within the converging nozzle its length changes and so does the length of the horizontal sides of a cell.

The distribution of the velocity and the density in the projectile are approximated by step functions of x that change over time. The boundary between two cells, which are also nodes at Figures 6.2 and 6.3, constitute a discontinuity of u and p functions. The collapse of such discontinuity results in the emanation of two waves moving along the two characteristics. The Riemannian invariants below are used to find the state of the fluid between the two waves:

$$\frac{dx}{dt} = u \pm \rho^{\frac{n-1}{2}} \tag{6.12}$$

$$u \pm \frac{2}{n-1}\rho^{\frac{n-1}{2}} = const \tag{6.13}$$

Where u and ρ are constant on the lateral sides 1-2 and 4-3 of each cell, and are calculated from a discontinuity of decomposition using equations of characteristics: the values at the following instance of time ($t+\tau$) are to be found.

A point of discontinuity, which is every node of the mesh, is a common point for the characteristic of the first family, second family, and the lateral side of the grid to which the point belongs to. Thus, from (6.12, 6.13) the following equations hold:

$$u_1 - \frac{2}{n-1}\rho_1^{\frac{n-1}{2}} = U - \frac{2}{n-1}Ro^{\frac{n-1}{2}} \tag{6.14}$$

$$u_2 - \frac{2}{n-1}\rho_2^{\frac{n-1}{2}} = U - \frac{2}{n-1}Ro^{\frac{n-1}{2}} \tag{6.15}$$

Using system (6.14, 6.15) the value of velocity and density at the lateral sides, U and Ro, can be determined by using formulas below where dt should be sufficiently small so that the characteristics do not intersect the lateral sides.

$$U = \frac{1}{2}\left[u_1 + u_2 - \frac{2}{n-1}\left(\rho_1^{\frac{n-1}{2}} - \rho_2^{\frac{n-1}{2}}\right)\right] \tag{6.16}$$

$$Ro = \left[-\frac{n-1}{4}(u_1 - u_2) + \frac{1}{2}\left(\rho_1^{\frac{n-1}{2}} + \rho_2^{\frac{n-1}{2}}\right)\right]^{\frac{2}{n-1}} \tag{6.17}$$

Using the values of U and Ro obtained in (6.16, 6.17) u and ρ can be related at the time instances t and $t+dt$ [1, 2]:

$$u^{m+1/2} = \frac{1}{\Delta_1}\left[u_{m+1/2}\Delta_2 - dt\left(c_{m+1} - c_m - U_{m+1}W_{m+1} + U_m W_m\right)\right] \tag{6.18}$$

$$\rho^{m+1/2} = \frac{1}{F_u \Delta_1}\left[F_l \rho_{n+1/2}\Delta_2 - dt\left(\left(RUF\right)_{m+1} - \left(RUF\right)_m - \left(RFW\right)_m + \left(RFW\right)_m\right)\right] \tag{6.19}$$

$$c_i = \frac{U_i^2}{2} + \frac{Ro_i^{n-1}}{n-1} \tag{6.20}$$

$$W_m = \left(x^m - x_m\right)/dt \tag{6.21}$$

Where: F_l, F_u, F_m, and F_{m+1} are the average values of nozzle cross-section area corresponding to the sides of a cell *1-4*, *2-3*, *1-2* and *3-4* respectively.

A computer code has been developed for the simulation of water cannon operation using this scheme (equations 6.16 – 6.21). A block of code modeling gunpowder combustion was also included in the program.

CHAPTER 7

SELECTIVE DEMINING [5]

This series of experiments had been performed with Oleg Petrenko and Veljko Samardzic under the supervision of Dr. E. Geskin. There is an evident need for an efficient mine neutralization device. This approach to neutralization of mines is different from conventional in sense that it promotes technology which enables destruction of mine without explosion, and can save lives lost during mine neutralization and/or those lost in mine related accidents. In order to simulate a real case of neutralizing a mine embedded in topsoil a composite target was designed. General schematic of mine simulated environment is shown on Figure 7.1. A mine was simulated by Aluminum cooking pot

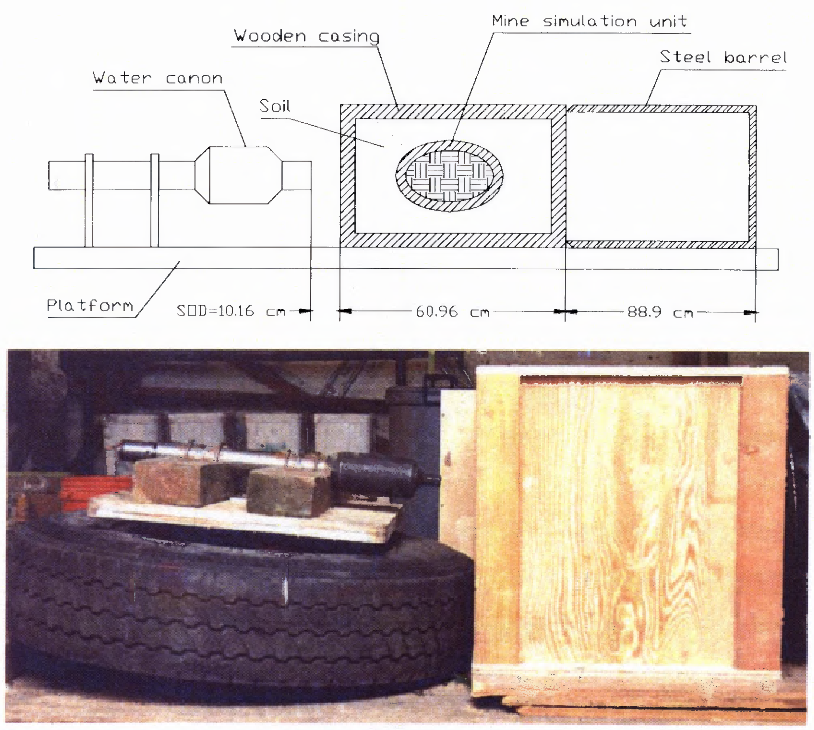

Figure 7.1 Selective demining experimental set up schematic and actual view of test site.

filled completely with wax. The pot was embedded in the densely packed top soil obtained from NJIT construction site. The soil was densely packed inside of 2 foot by 2foot by 2foot wooden containers, the walls of which are made of 3/4 inch thick A-grade plywood panels glued and nailed into 1" deep grooves of 3.5"x3.5"lumber. As a result a strong and solid structure of the container was obtained which can be depicted from photographs taken before and after the experiments. After completed packing of each container top panel was nailed to the stricture by 36 nails. The mine simulation unit was placed in the center of the wooden container. In each of the two attempts, described below there was 10.16 cm stand of distance between the nozzle and the wooden container, and a 55 gallon, 88.9 cm long and 0.90 mm thick steel barrel was placed behind the wooden container. The barrel was coated on the inside and painted on the inside.

Figure 7.2 Damage of front panel (left) and back panel (right), caused by action of 230 g water-projectile in the first attempt.

The first attempt was performed by use of 230 grams of water which were propelled by combustion of 70.655 grams of a rifle powder. As a result, all obstacles placed in front of the cannon were pierced. Front wood panel (Figure 7.2-left) has an opening of oval shape with large axes of 58mm and small axes of 33mm.

About 2/3 of surface layer of the front panel were removed by projectile impact indicating radial flow of water in the direction of large axes of the opening. The shape of the opening and the direction of the material removal from the front panel indicate 3-dimensional instability in the flow of the projectile. Aluminum pot as a mine simulation unit was pierced in the same manner as metal plates (Figure 7.3). Two bottle neck

Figure 7.3 Damage of mine simulation unit caused by 230 g water-projectile in the first attempt.

deformed volume segments were formed, one at the entering site of the projectile into the pot and another at the exiting site of the projectile from the pot. The entering bottle neck segment has an irregular oval shape with 59.13mm large axes and 56.59mm small axes. and the depth of 30.35mm. Exiting bottleneck has also an oval shape with 74mm large axes and 47.98mm small axes. This large difference in size of axes indicates existence of an intensive instability within the flow of the projectile at the exiting site, which has six large primary cracks that reach to the base of the bottleneck. There is a trace of projectile's path through the wax content of the pot indicating two pulses of the projectile during piercing of the pot, which appears to be of compatible intensity and duration. The trace of the first pulse spreads between the entering opening and ends around the midpoint of the pot in the direction of the flow. The trace of the second pulse spreads between the end of the first pulse and the exiting bottleneck base. Maximal spreading diameter of the projectile inside of the pot was around 88.9mm, it is the same for both pulses. The back panel of the wooden container was pierced in the manner indicating significant radial spreading of the projectile. A deformed rectangular wide base area is 14cm x20cm in size and has central pierced area where lignin matrix and cellulose fibers were ruptured from the impact (Figure 7.1). The rest of the deformed area has numerous multidirectional cracks. The base of the steel barrel which was located 88.9cm away from the back panel of the wooden container was pierced in five spots. Four of these openings are located within 8cm diameter and the fifth is 6cm away from the central circular area of the impact. The appearance of this impact site indicates additional spreading of the projectile as it gets away from the nozzle. The appearance of anterior of the barrel gives imprint of deflected flow of the water where radial and back flow steam lines can be depicted from corrosion nucleation cites which appeared everywhere where coating was removed.

The second mine simulation attempt was performed by using 230 grams of water which was propelled by combustion of 64.683 grams of rifle powder. In this case, all obstacles placed in front of the cannon were pierced as well. Front wood panel has an opening of irregular oval shape with large axes of 65mm and small axes of 45mm (Figure 7.4 -left). The radial upward water flow was removed surface layers from the panel, and created an area roughly twice the size of the area of the opening. This material removal

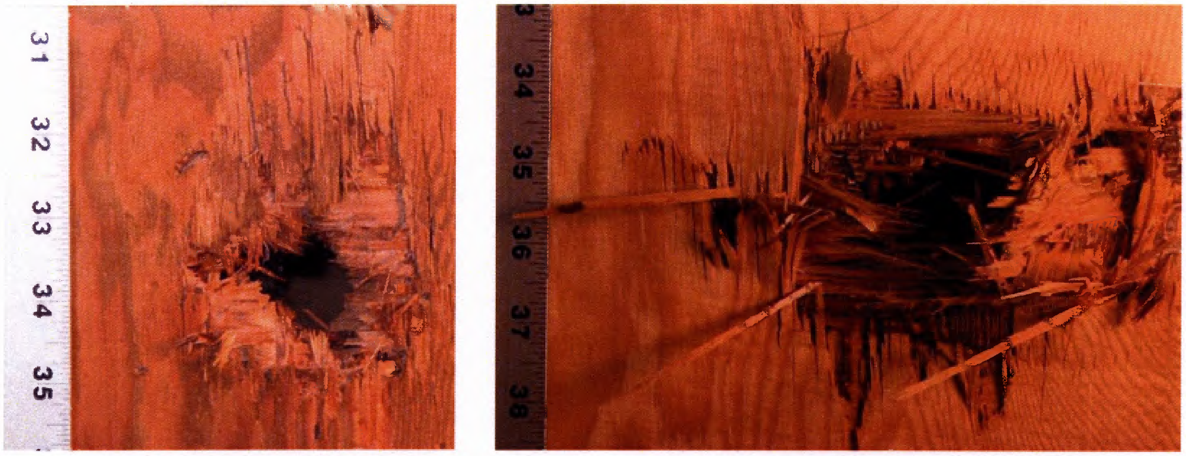

Figure 7.4 Damage of front panel (left) and back panel (right) caused by action of 230 g water-projectile in the second attempt.

took place in the direction of large axes of the opening. The shape of the opening and the direction of the material removal from the front panel indicate 3-dimensional instability in the flow of the projectile as well. Aluminum pot was pierced in the same manner as in the first attempt (Figure 7.5). Two bottle neck deformed volume segments were formed, one at the entering site of the projectile into the pot and another at the exiting site of the projectile from the pot. The entering bottle neck segment has slightly oval shape with 46.68 mm large axes and 43.33 mm small axes, and depth of 36.27 mm. Exiting bottleneck has also oval shape with 46mm large axes and 37.29 mm small axes, and the depth of 36.27 mm. Significant difference in size of axes indicates existence of instability within the flow of the projectile at the exiting site. As in the first attempt, the opening has six large primary cracks that reach to the base of the bottleneck. A clear trace of projectile's path through the wax content of the pot indicates a single pulse of the projectile during piercing of the pot, and the trace of the pulse spreads between the entering opening and exiting opening. Maximal spreading diameter of the projectile was 152.4 mm, and it is located around the midpoint of the pot in the direction of the flow. In this attempt, the back panel of the wooden container was pierced in the same manner as in the first attempt which indicates a significant radial spreading of the projectile. Rectangular wide base deformed area is 20cm by 14cm in size, and has heavily ruptured central pierced area where lignin matrix and cellulose fibers were ruptured from the impact area. The rest of the deformed area has numerous multidirectional cracks as well. The base of the steel barrel was pierced and single opening was created.

Figure 7.5 Damage of mine simulation unit caused by 230 g water projectile in the second attempt.

7.1 Concrete Demolition

To demonstrate a concrete demolition two attempts were performed. In each attempt a composite target made of four 10.16cm (4x4 inch) thick solid concrete blocks was mounted on a target holder at the stand of distance of 2cm (Figure 7.1.1).

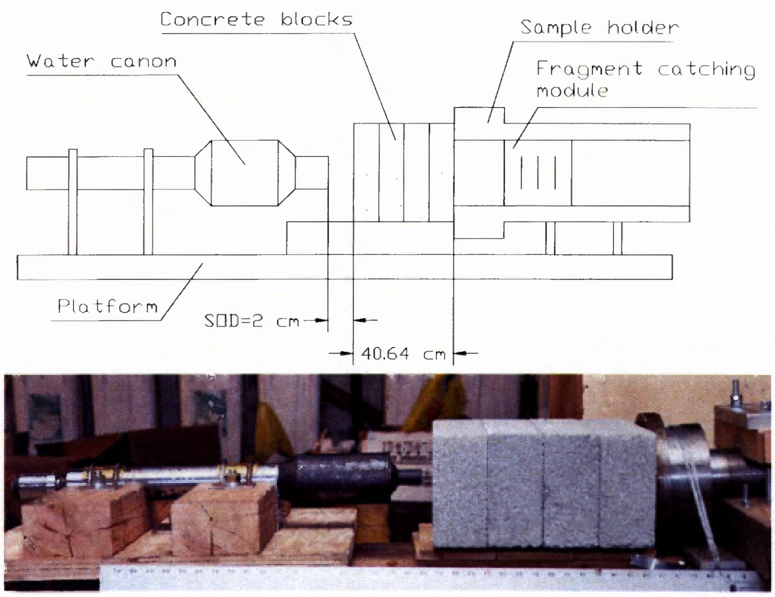

Figure 7.1.1 Concrete demolition experimental set up schematic and actual view of test site.

First attempt was performed by impact of 230 g of water propelled by combustion of 66.826g of rifle powder. Explosion like failure of the target took place. As a result, high level of destruction was achieved and the concrete target was completely shattered into fragments ranging in size between sand grain particle as minimal size and 20x15x10 cm as a maximal size (Figure 7.1.2).

Identical set up was used in the second attempt except for amount of rifle powder which was 64.163 g. The failure of the target and the results of the second attempt looked identical by all criteria used for characterization of the results. The results from both experiments comply with the results obtained earlier on concrete demolition investigation which confirms good repeatability of the operation. Due to porosity of concrete and the nature of failure, it can be said that simultaneous multiple crack initiation took place and further lead by high rate chain crack propagation which resulted in explosion like failure.

Figure 7.1.2 Concrete demolition caused by 230 g water projectile.

CHAPTER 8

CONCLUSION

The performed studies demonstrated feasibility of the use of the high speed impulsive jets for a wide range of technological operations, such as the structure demolition, explosive neutralization, material processing, and others. Numerical modeling of projectile formation provides the necessary preprocessing data for analysis, design and further study of the water cannon. The research has indicated that the nozzle geometry has significant effect on the device operation and must be determined from the conditions of the process optimization, and possibly, the cannon may have a curvilinear axial cross section. At the same time, water cannon might be not necessarily a solid body but may consist of separate parts. Various kinds of nozzles could be attached to the barrel depending on industrial or military task being executed. The optimization of the available data will improve substantially the efficiency of the water cannon, as well as other jet technologies. The major concern in the application of the optimization technique is a lack of information about the physics of the process, but even processing of low quality information enables to receive the important guidance to the process improvement.

APPENDIX A

PRESSURE AND VELOCITY DISTRIBUTION PLOTS WITH DIFFERENT WATER LOADS

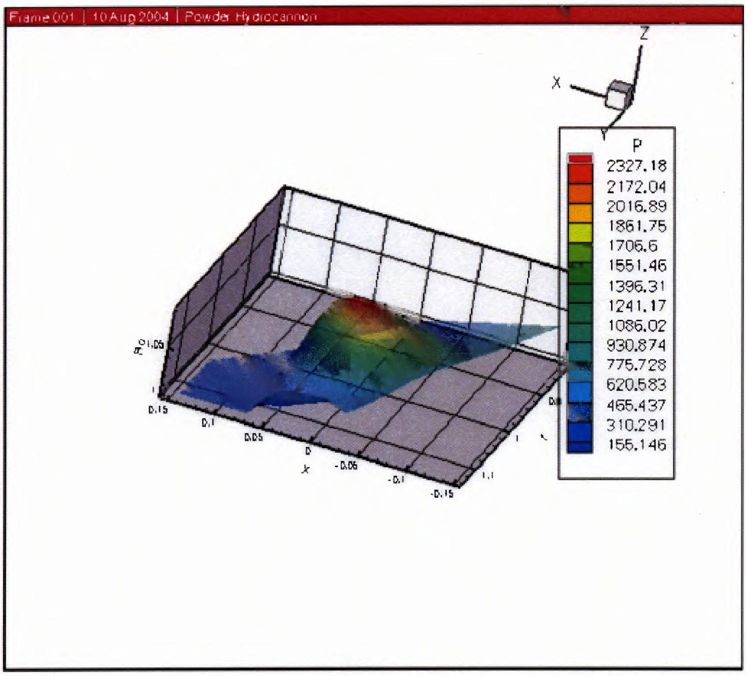

Figure A.1 Pressure distribution plot with 100 g water projectile.

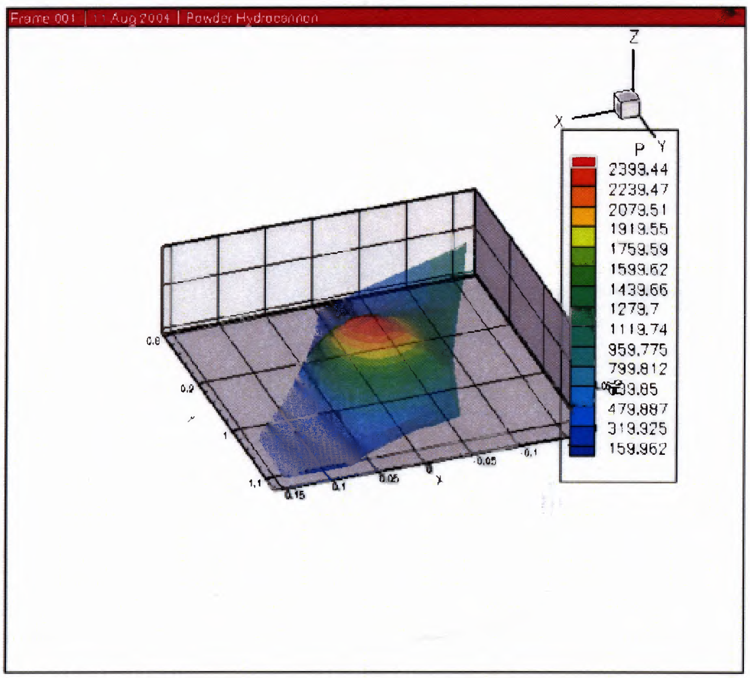

Figure A.2 Pressure distribution plot with 110.337 g water projectile.

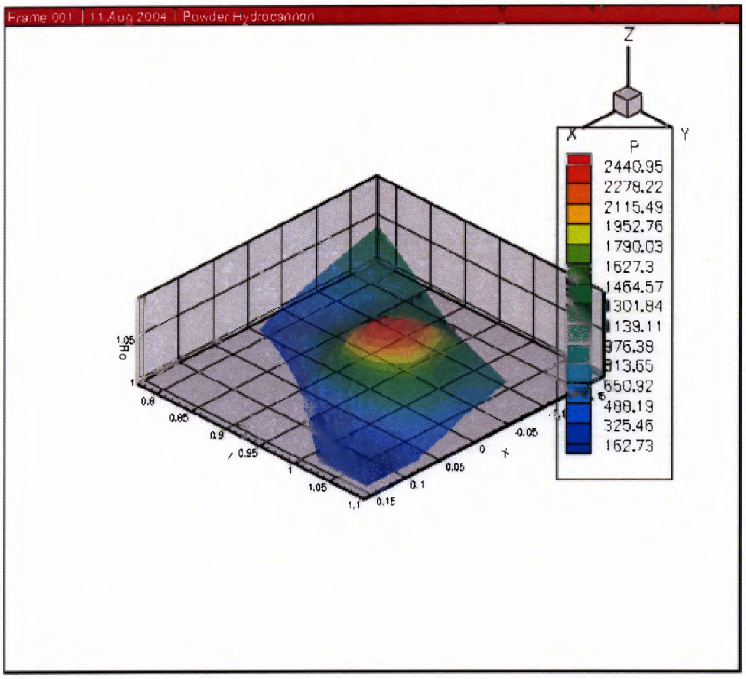

Figure A.3 Pressure distribution plot with 120.674 g water projectile.

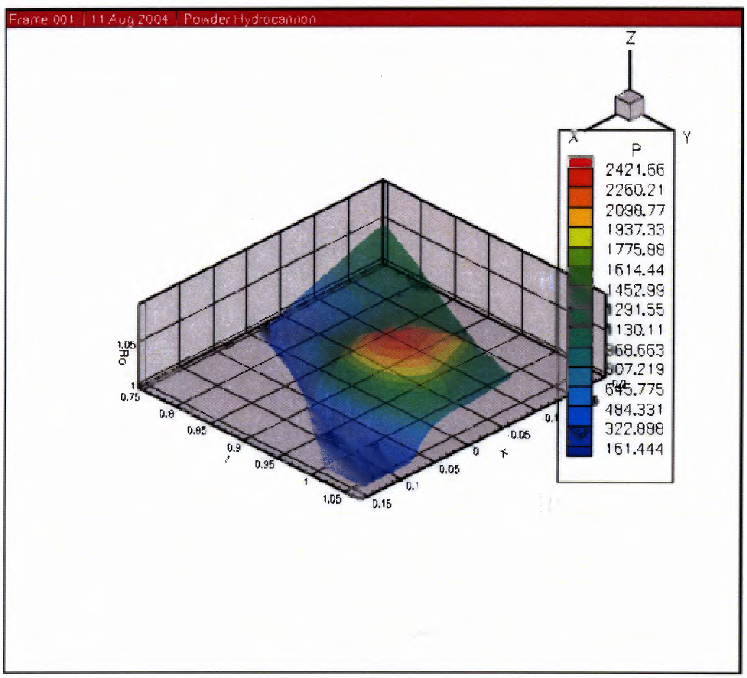

Figure A.4 Pressure distribution plot with 131.012 g water projectile.

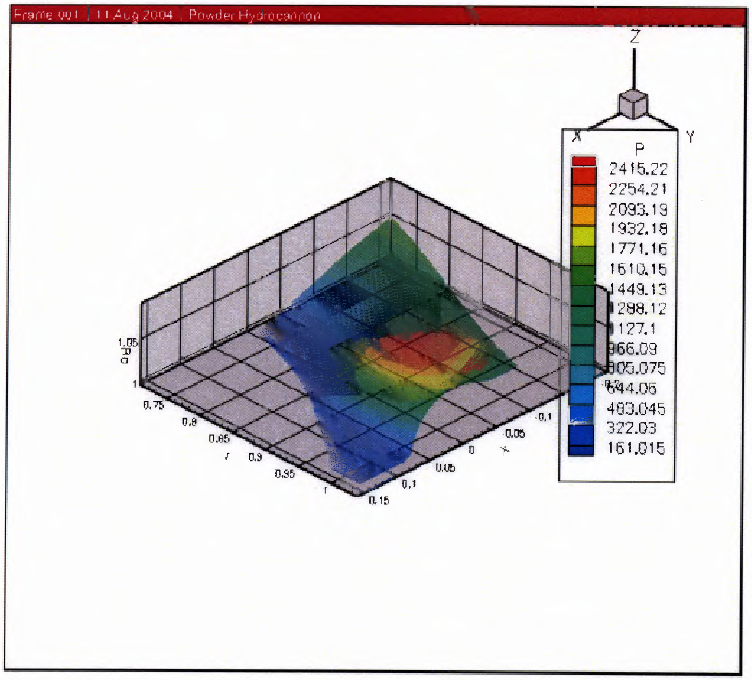

Figure A.5 Pressure distribution plot with 141.349 g water projectile.

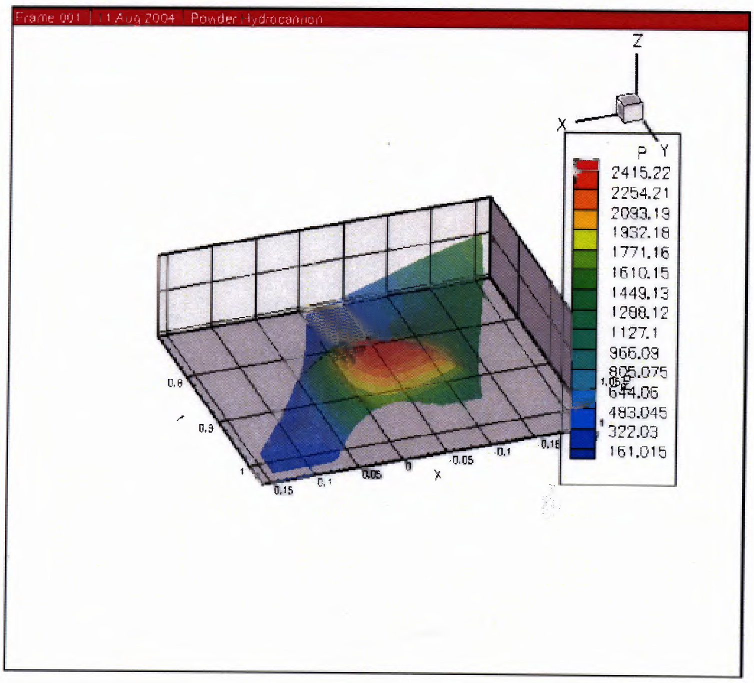

Figure A.6 Pressure distribution plot with 151.686 g water projectile.

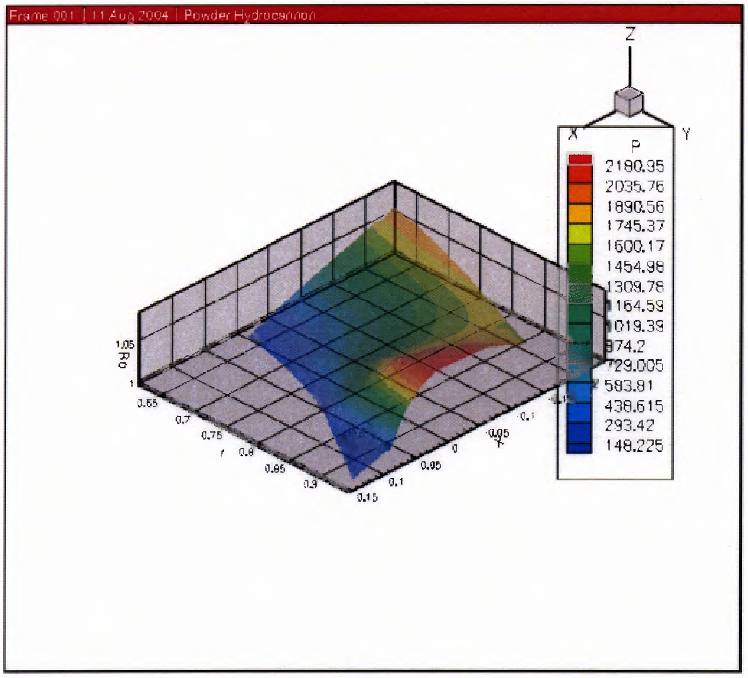

Figure A.7 Pressure distribution plot with 162.023 g water projectile.

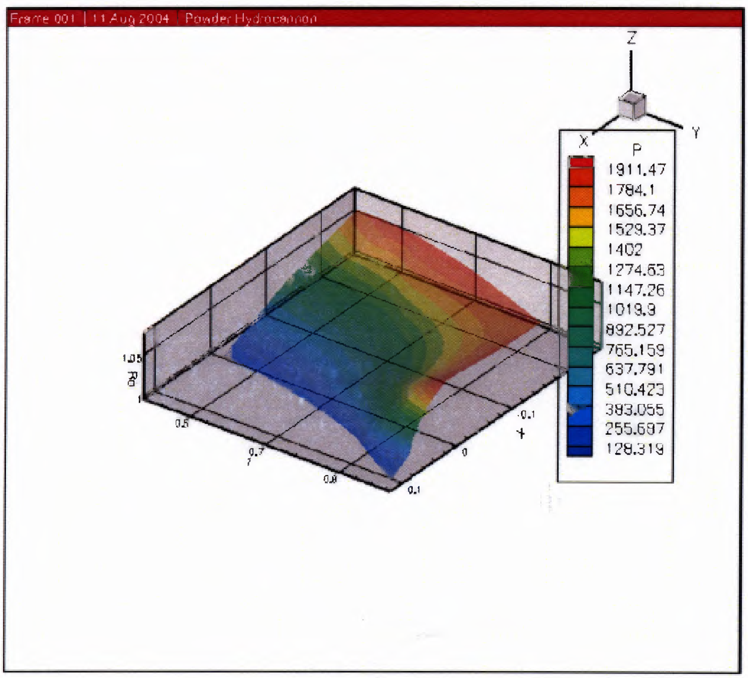

Figure A.8 Pressure distribution plot with 172.36 g water projectile.

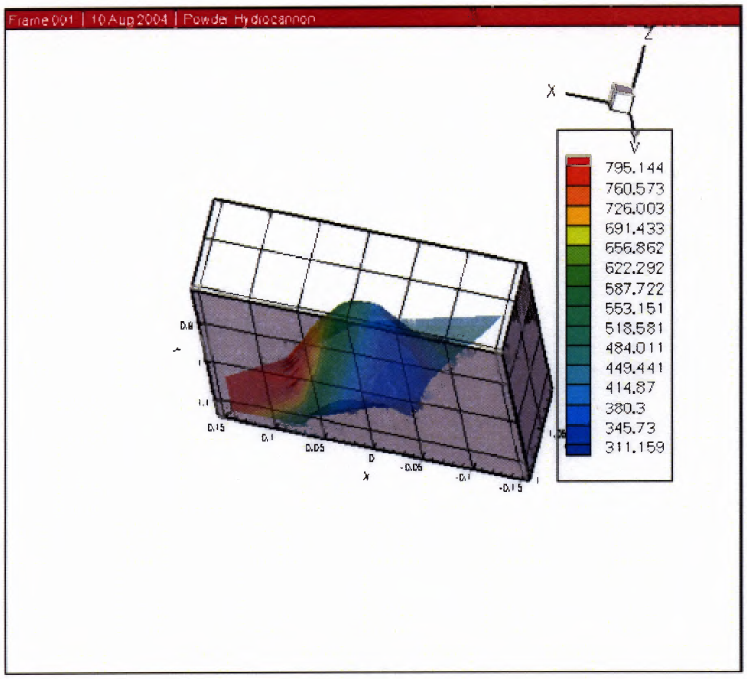

Figure A.9 Velocity distribution plot with 100 g water projectile.

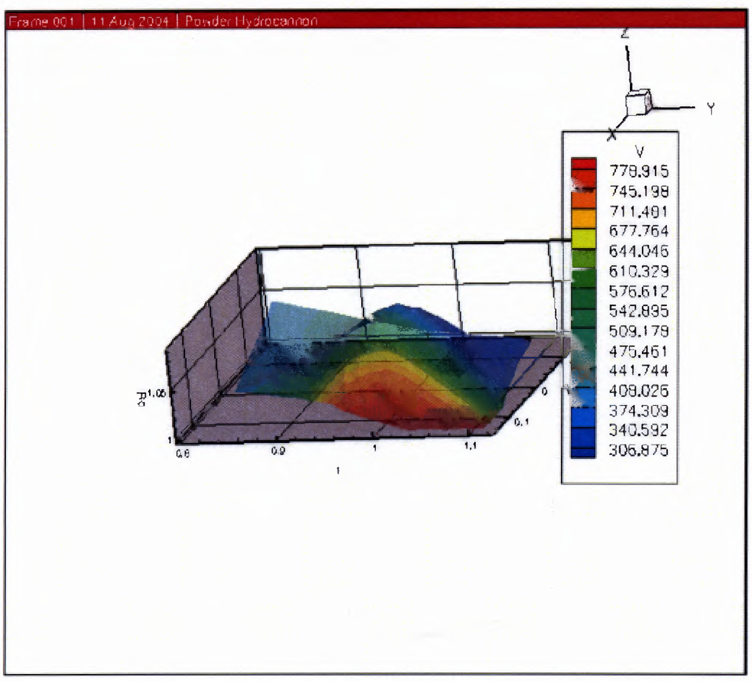

Figure A.10 Velocity distribution plot with 110.337 g water projectile.

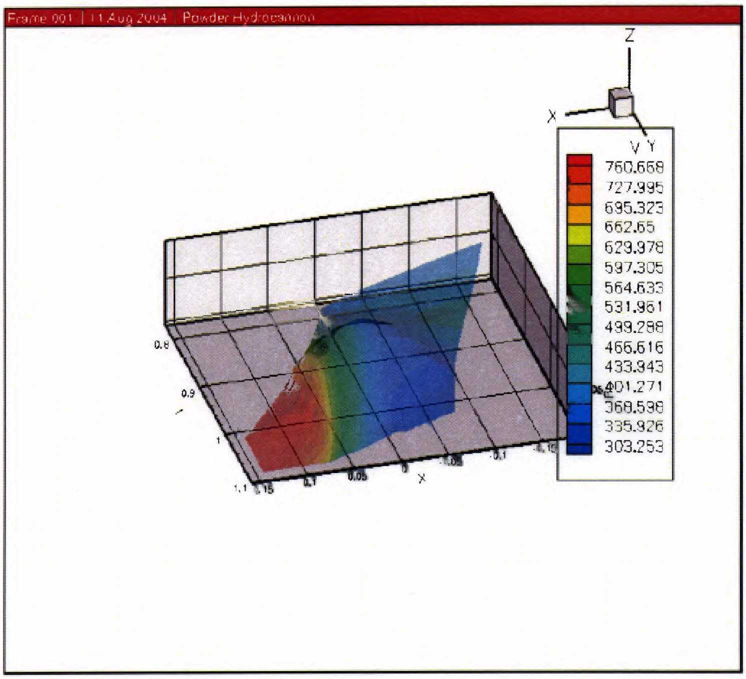

Figure A.11 Velocity distribution plot with 120.674 g water projectile.

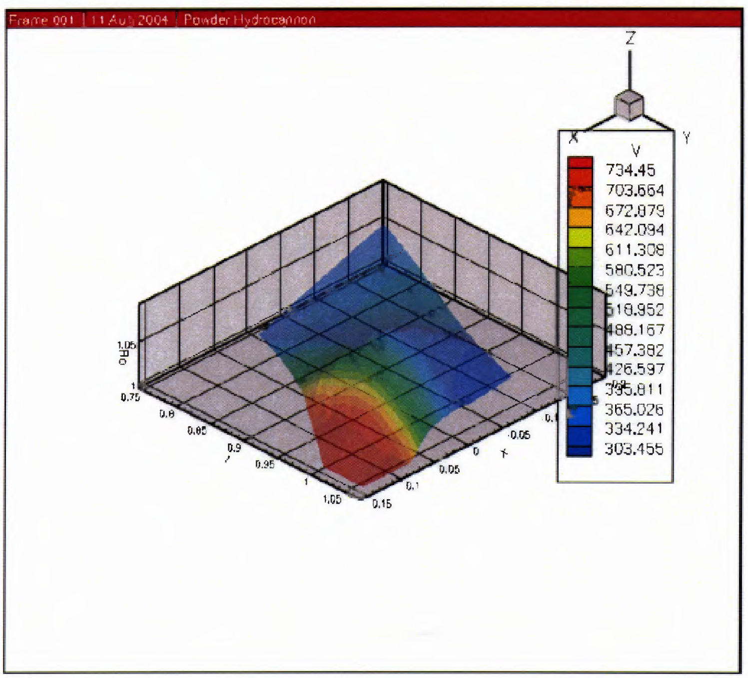

Figure A.12 Velocity distribution plot with 131.012 g water projectile.

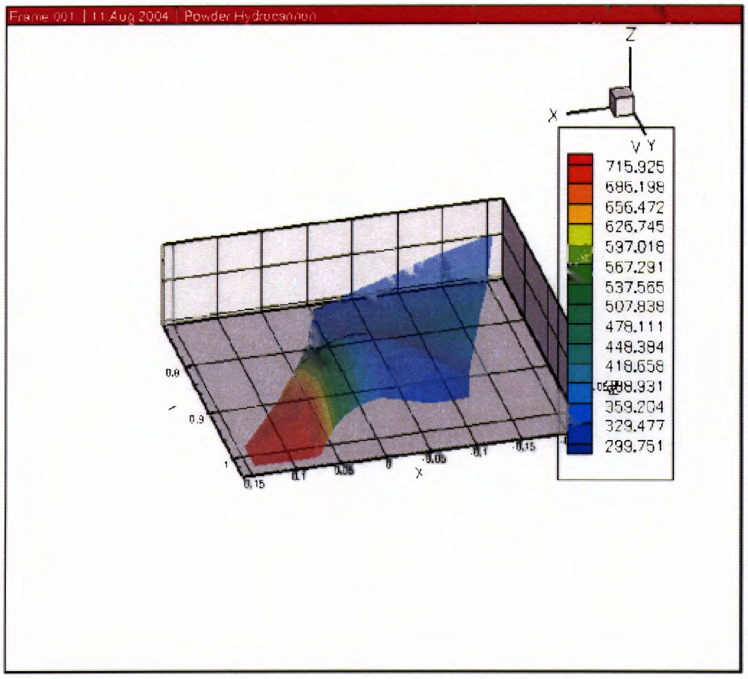

Figure A.13 Velocity distribution plot with 141.349 g water projectile.

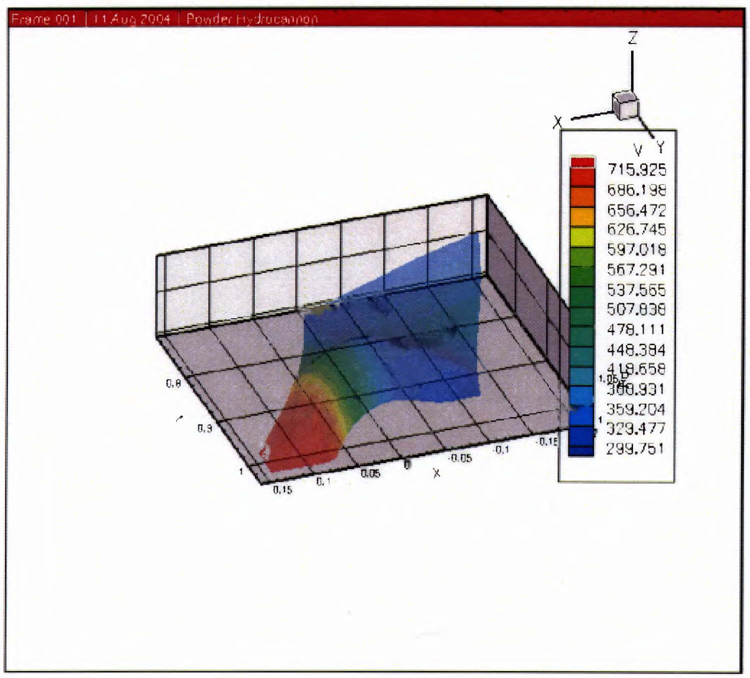

Figure A.14 Velocity distribution plot with 151.686 g water projectile.

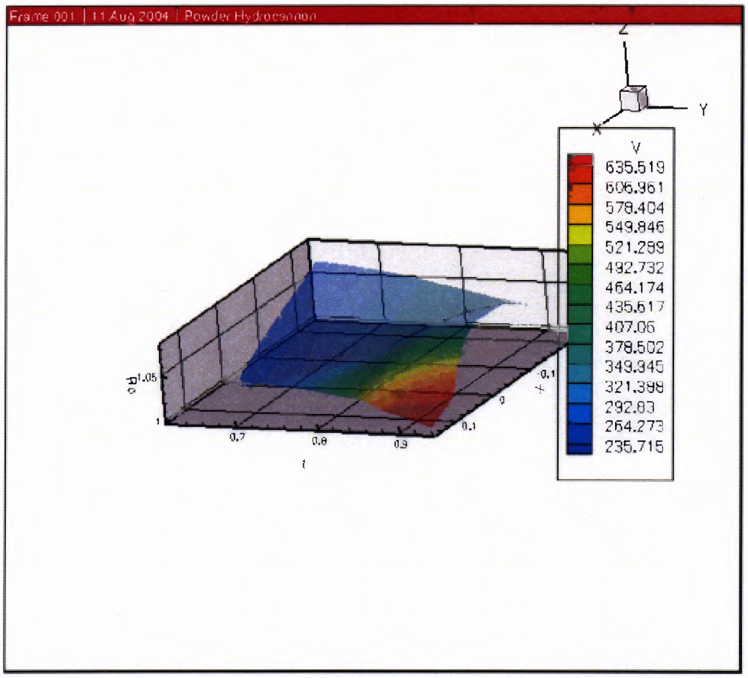

Figure A.15 Velocity distribution plot with 162.023 g water projectile.

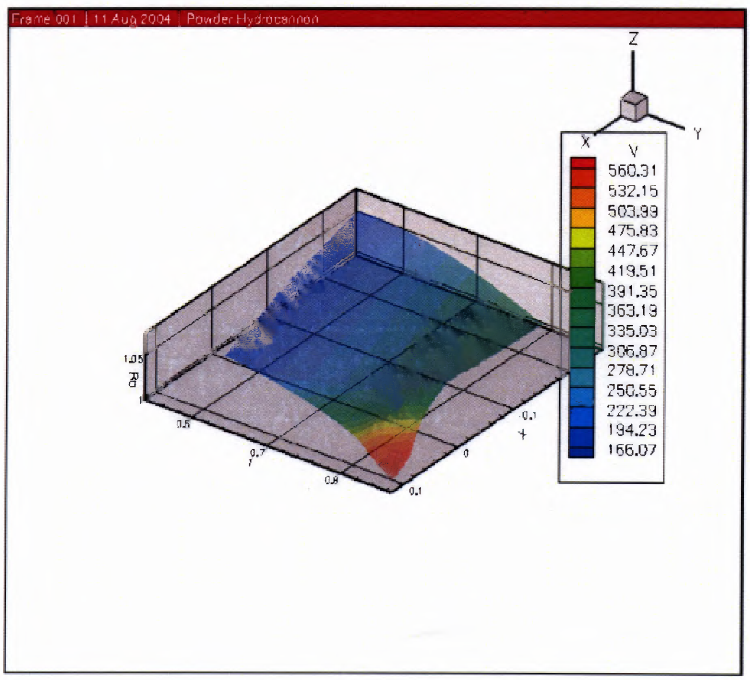

Figure A.16 Velocity distribution plot with 172.36 g water projectile.

APPENDIX B

IMPULSE INTEGRAL VERSUS WATER LOAD DISTRIBUTION PLOTS WITH DIFFERENT NOZZLE CONE LENGTHS

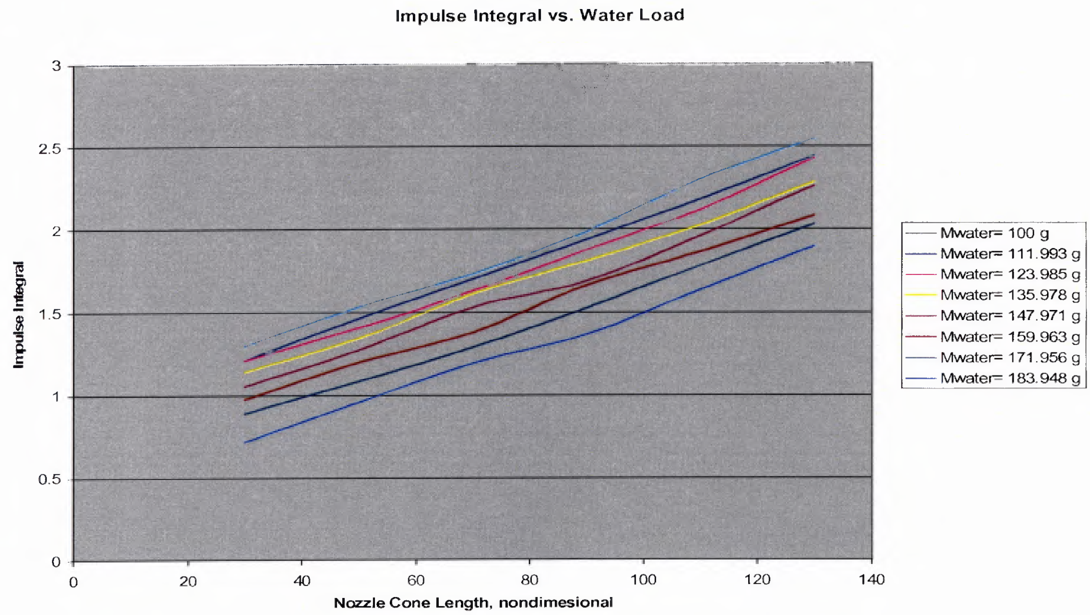

Figure B.**1** Impulse integral versus water load distribution plot with L_{bar}=280e-3, D_n2=5e-3, and D_n1=30e-3.

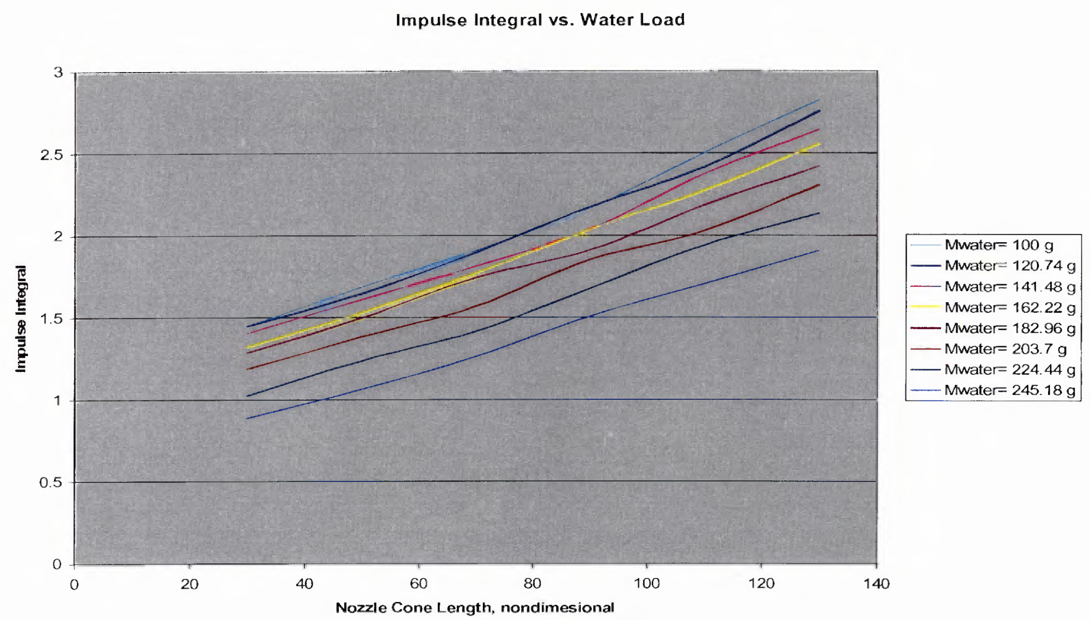

Figure B.**2** Impulse integral versus water load distribution plot with L_{bar}=380e-3, D_n2=5e-3, and D_n1=30e-3.

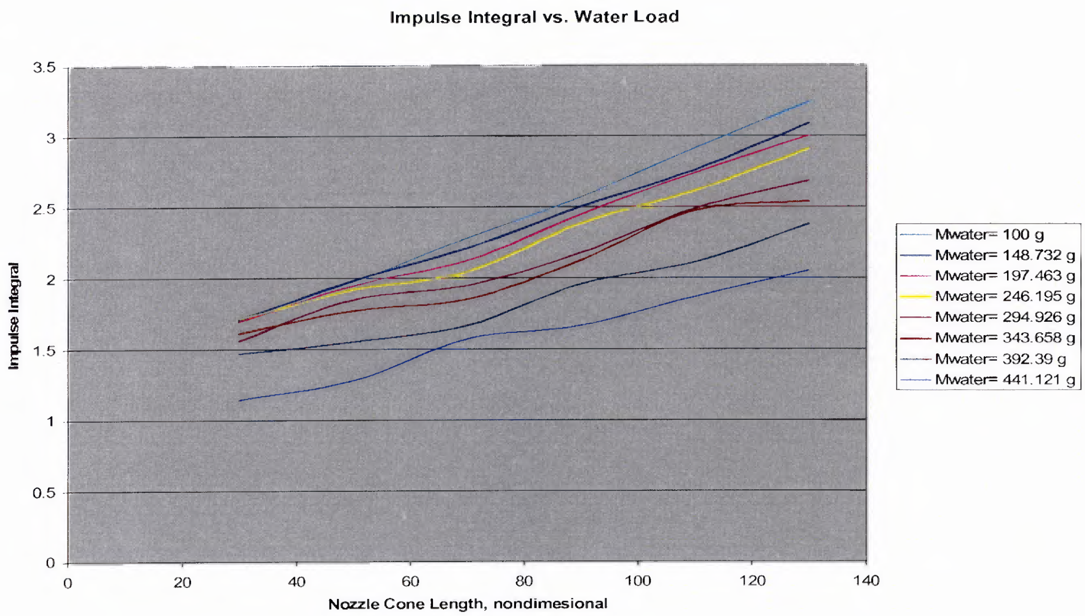

Figure B.3 Impulse integral versus water load distribution plot with L_{bar}=700e-3, D_n2=5e-3, and D_n1=30e-3.

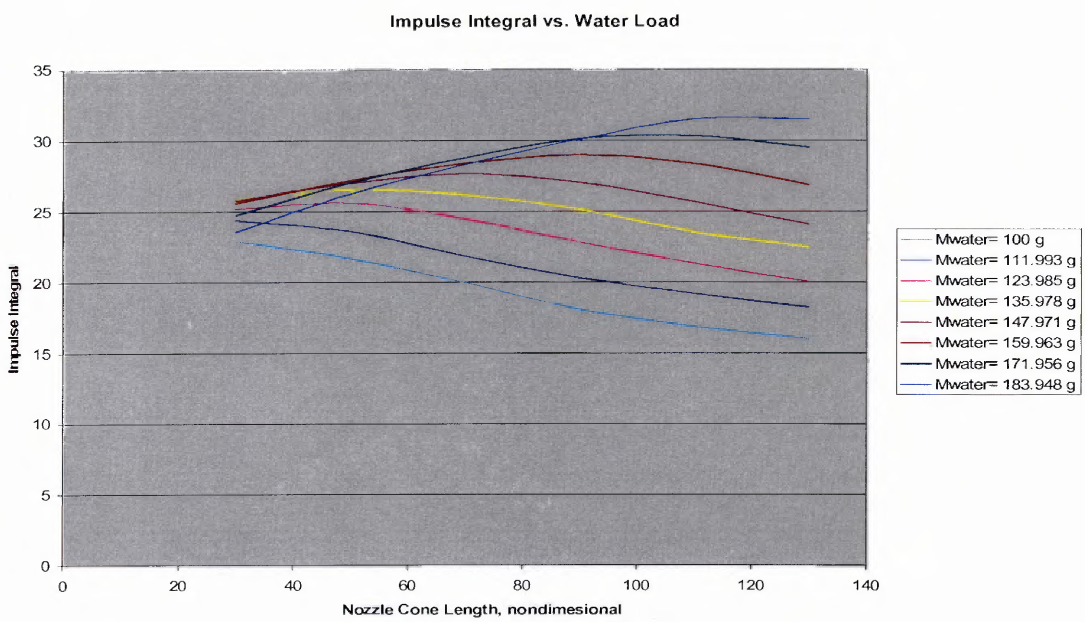

Figure B.4. Impulse integral versus water load distribution plot with L_{bar}=280e-3, D_n2=15e-3, and D_n1=30e-3.

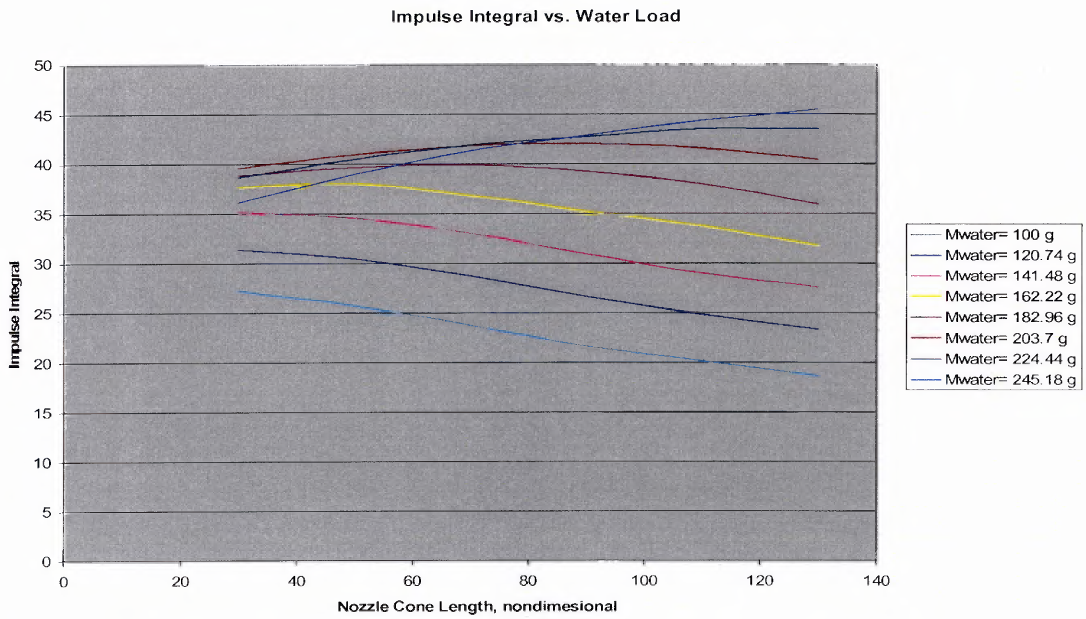

Figure B.5 Impulse integral versus water load distribution plot with L_{bar}=380e-3, D_n2=15e-3, and D_n1=30e-3.

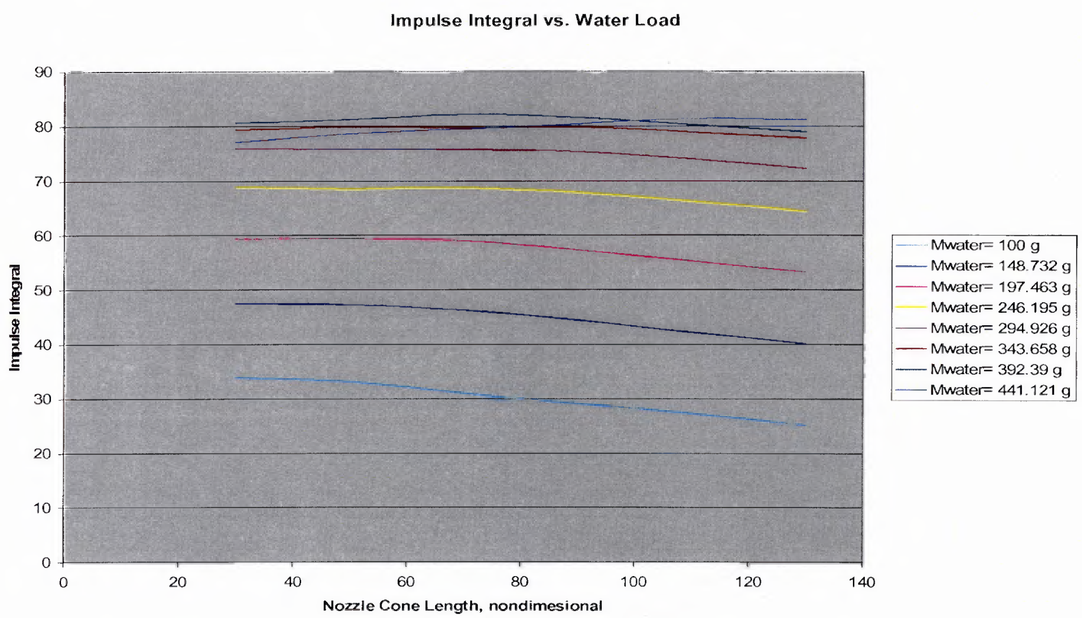

Figure B.6 Impulse integral versus water load distribution plot with L_{bar}=700e-3, D_n2=15e-3, and D_n1=30e-3.

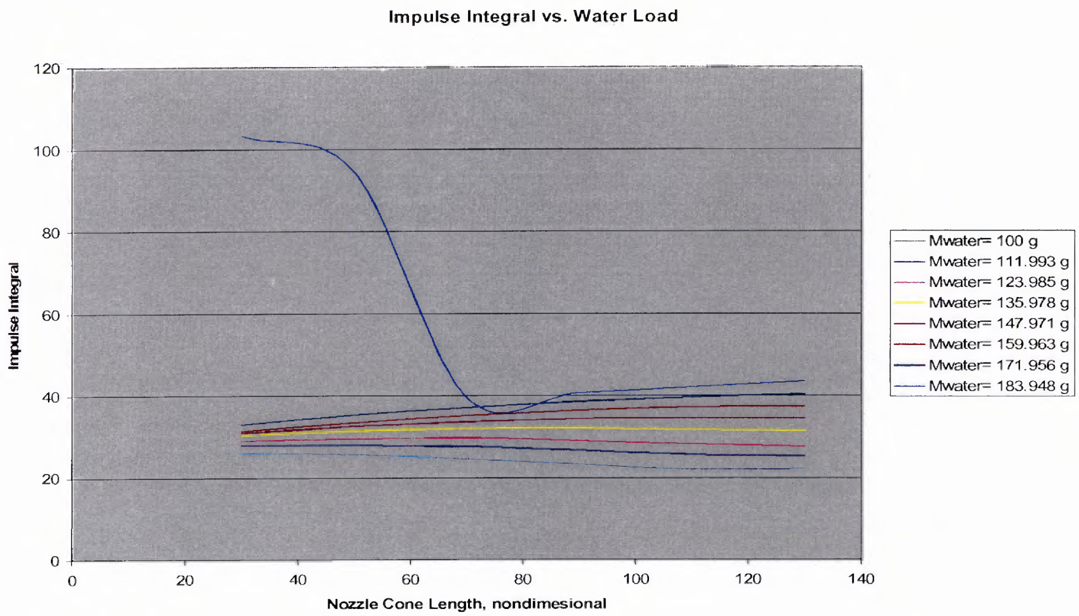

Figure B.7 Impulse integral versus water load distribution plot with L_{bar}=280e-3, D_n2=20e-3, and D_n1=30e-3.

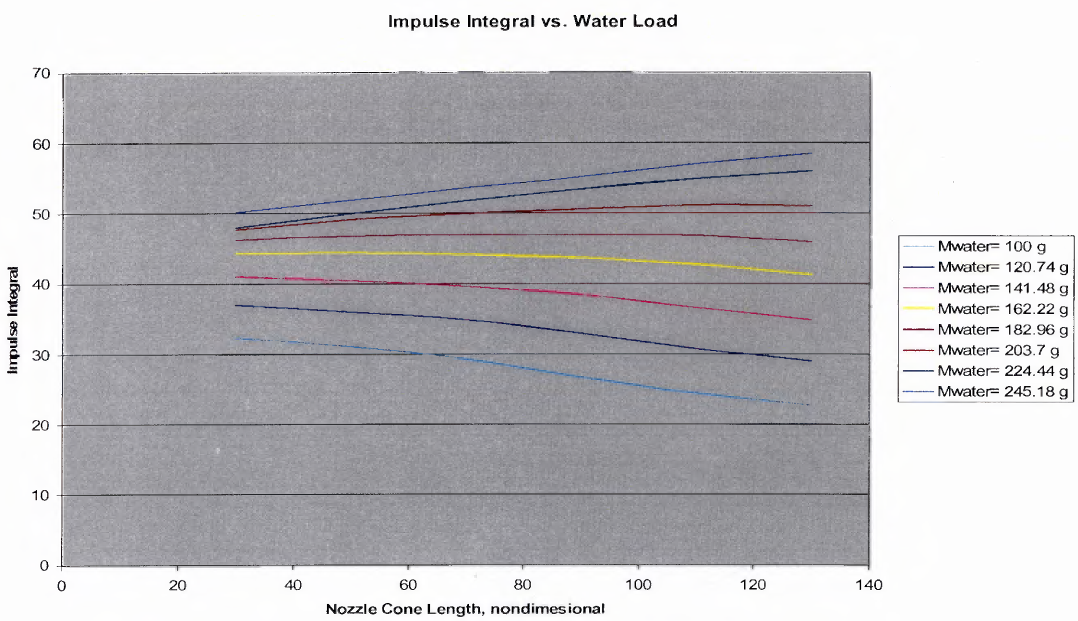

Figure B.8 Impulse integral versus water load distribution plot with L_{bar}=380e-3, D_n2=20e-3, and D_n1=30e-3.

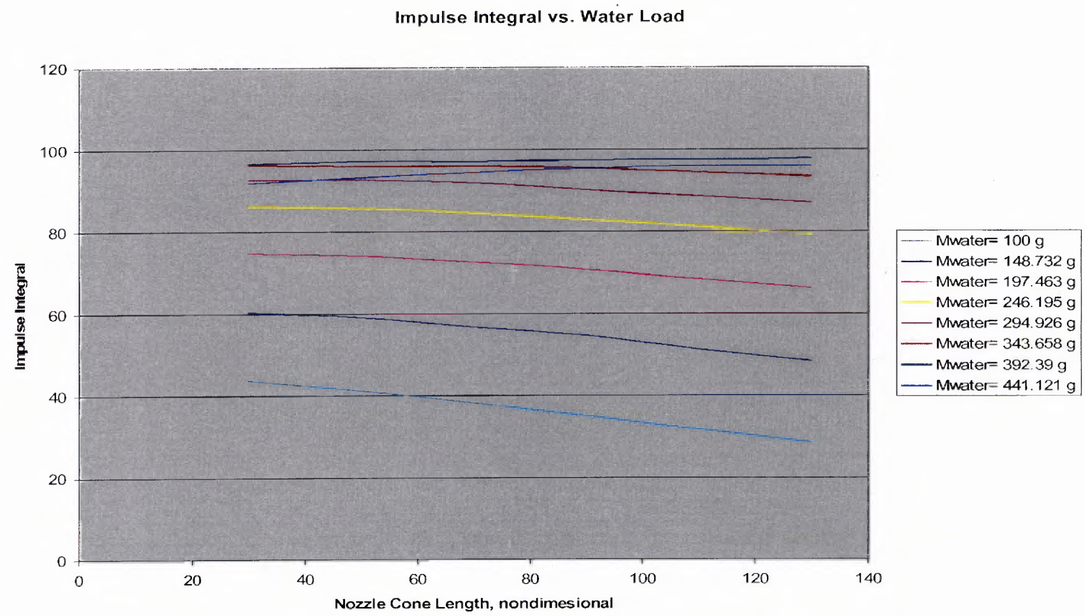

Figure B.**9** Impulse integral versus water load distribution plot with L_{bar}=700e-3, D_n2=20e-3, and D_n1=30e-3.

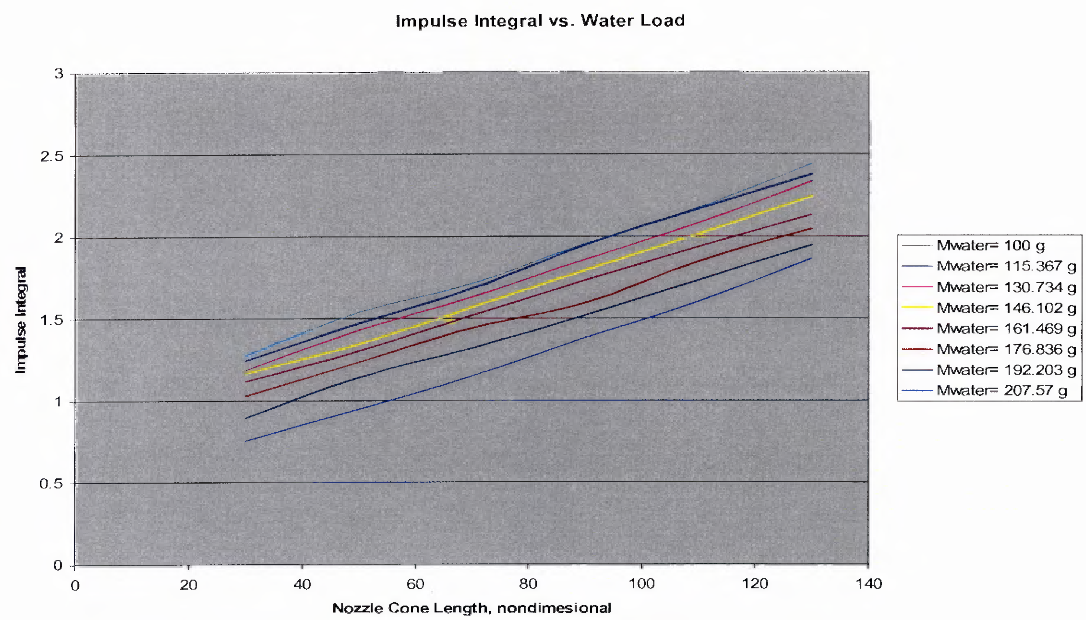

Figure B.**10** Impulse integral versus water load distribution plot with L_{bar}=280e-3, D_n2=5e-3, and D_n1=32e-3.

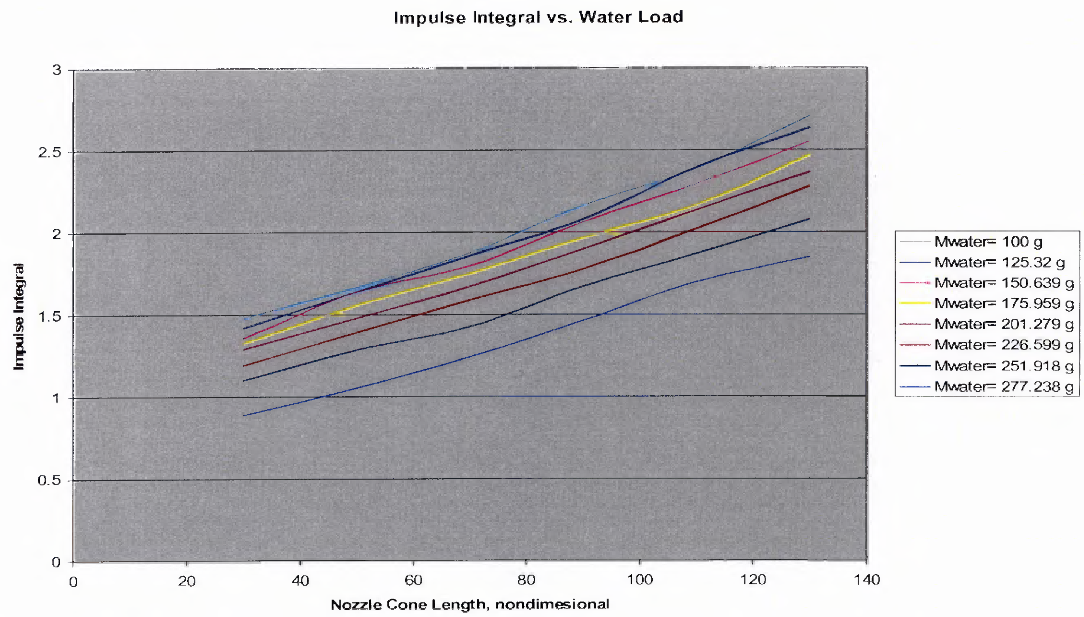

Figure B.**11** Impulse integral versus water load distribution plot with L_{bar}=380e-3, D_n2=5e-3, and D_n1=32e-3.

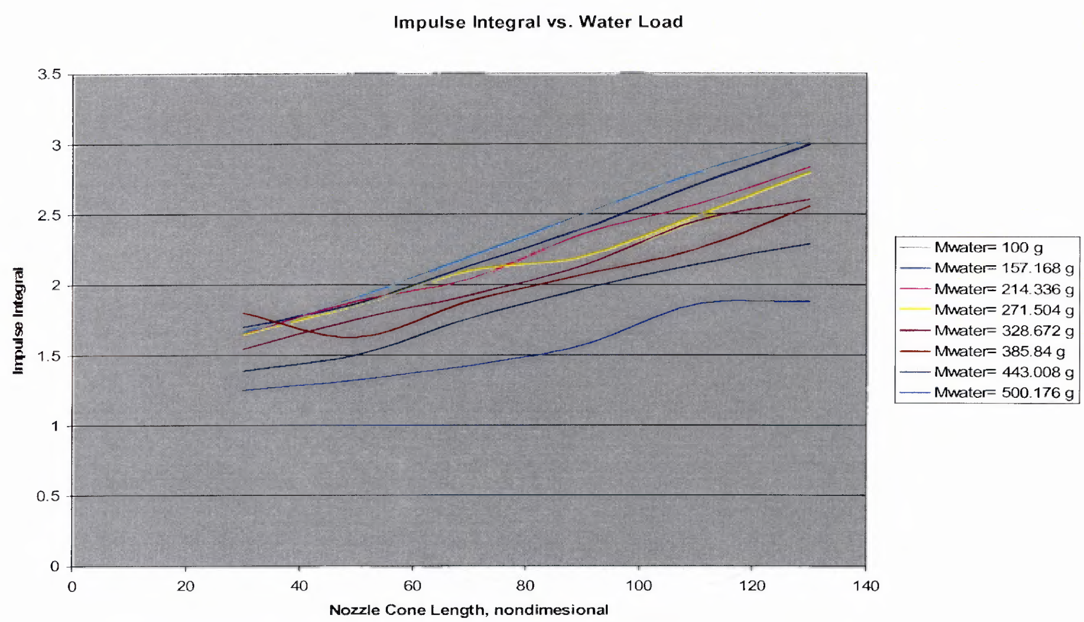

Figure B.**12** Impulse integral versus water load distribution plot with L_{bar}=700e-3, D_n2=5e-3, and D_n1=32e-3.

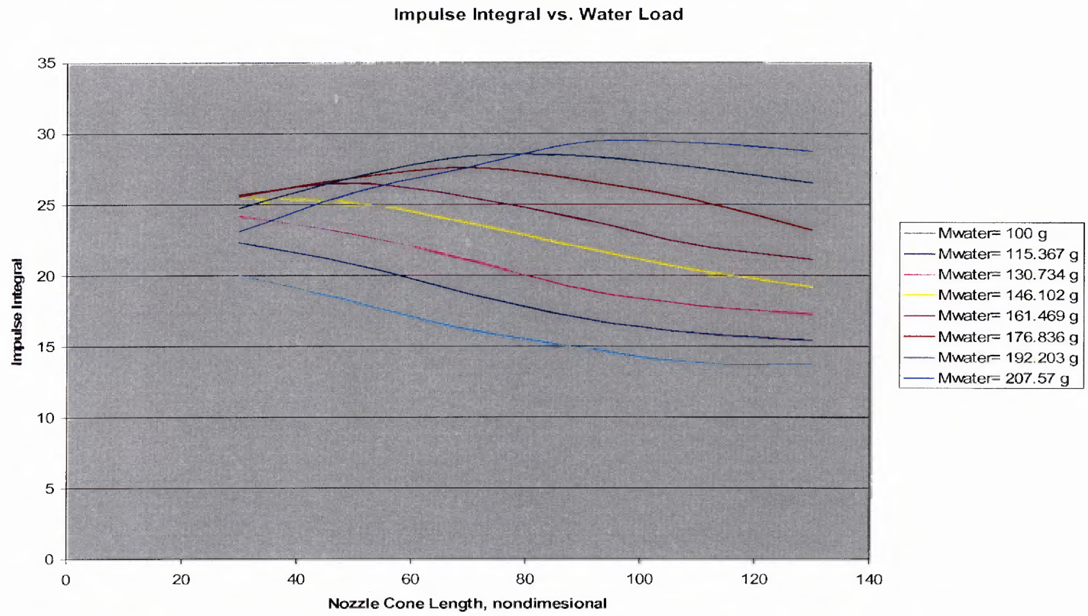

Figure B.13 Impulse integral versus water load distribution plot with L_{bar}=280e-3, D_n2=15e-3, and D_n1=32e-3.

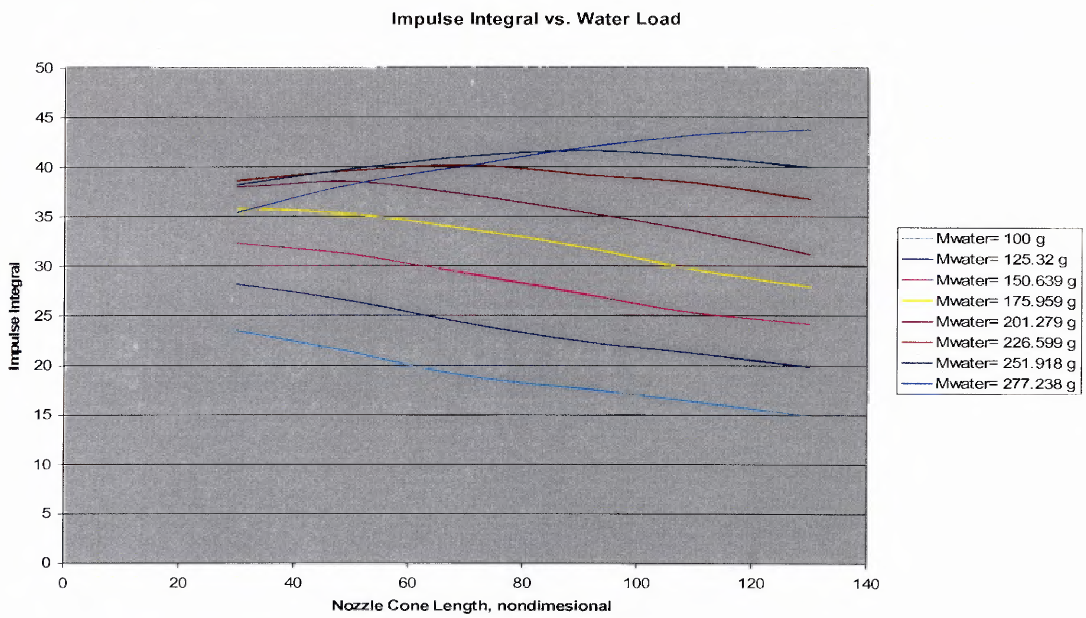

Figure B.14 Impulse integral versus water load distribution plot with L_{bar}=380e-3, D_n2=15e-3, and D_n1=32e-3.

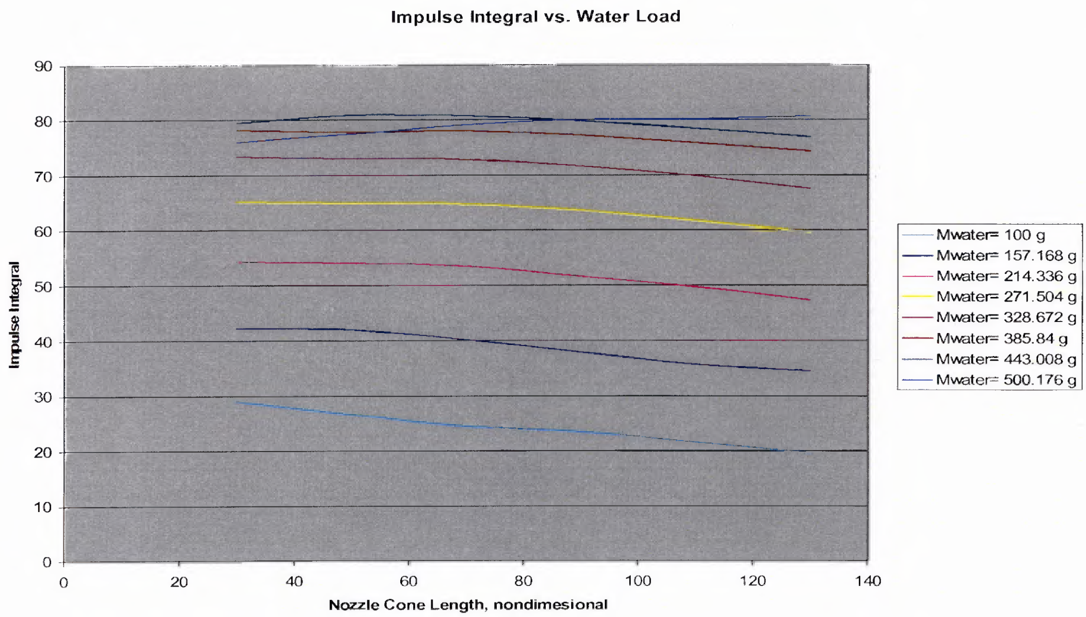

Figure B.**15** Impulse integral versus water load distribution plot with L_{bar}=700e-3, D_n2=15e-3, and D_n1=32e-3.

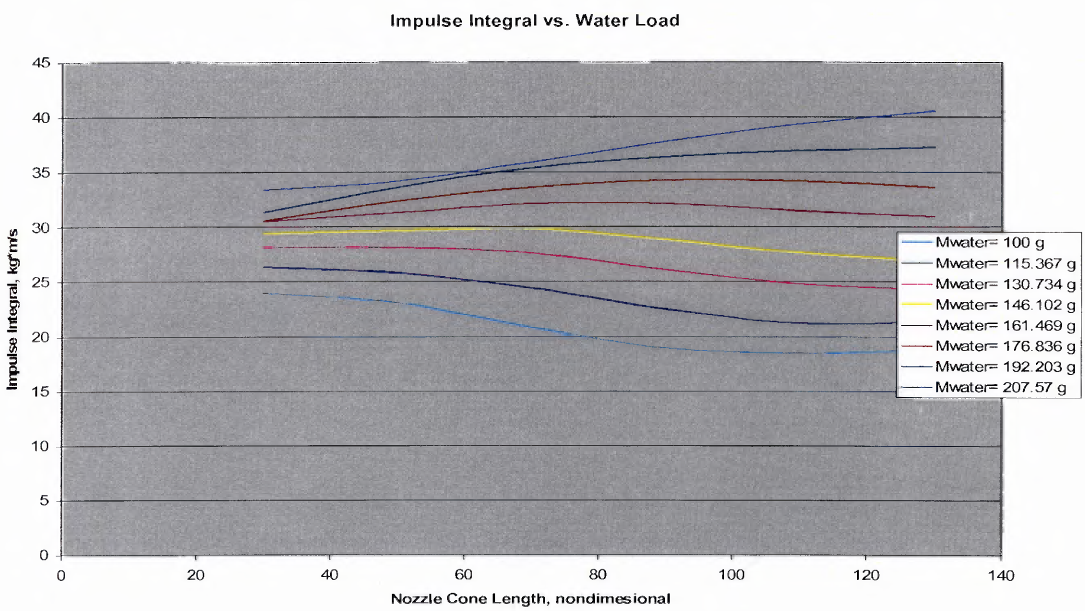

Figure B.**16** Impulse integral versus water load distribution plot with L_{bar}=280e-3, D_n2=20e-3, and D_n1=32e-3.

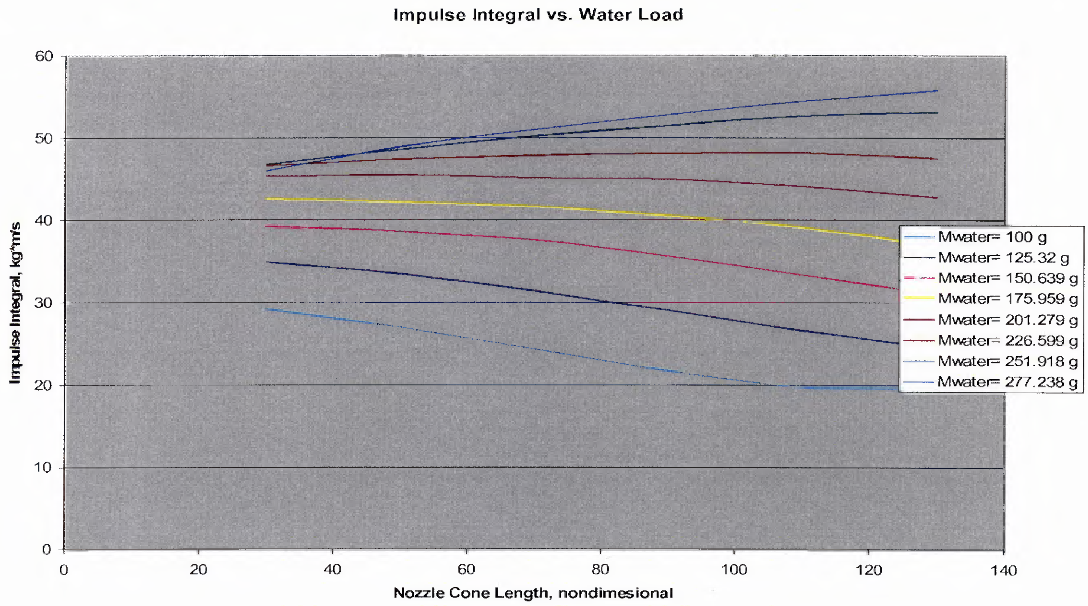

Figure B.17 Impulse integral versus water load distribution plot with L_{bar}=380e-3, D_n2=20e-3, and D_n1=32e-3.

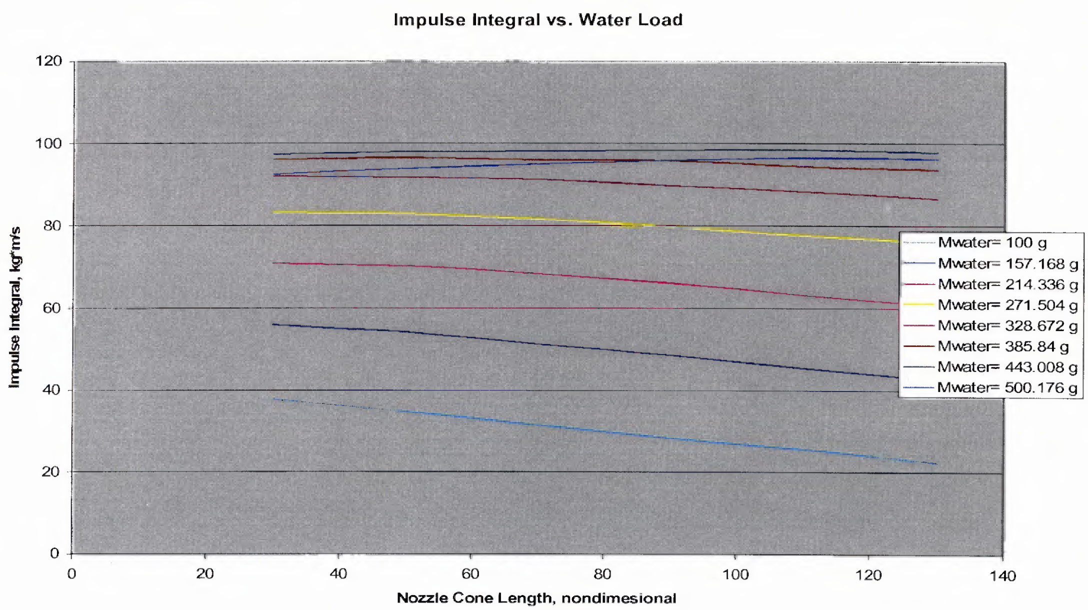

Figure B.18 Impulse integral versus water load distribution plot with L_{bar}=700e-3, D_n2=20e-3, and D_n1=32e-3.

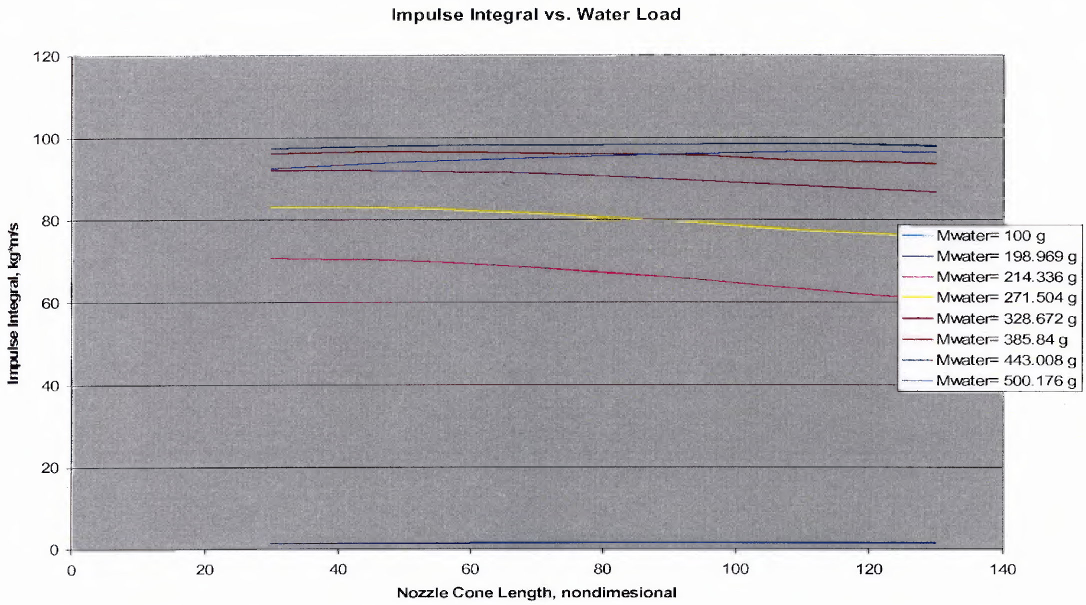

Figure B.19 Impulse integral versus water load distribution plot with L_{bar}=280e-3, D_n2=5e-3, and D_n1=64e-3.

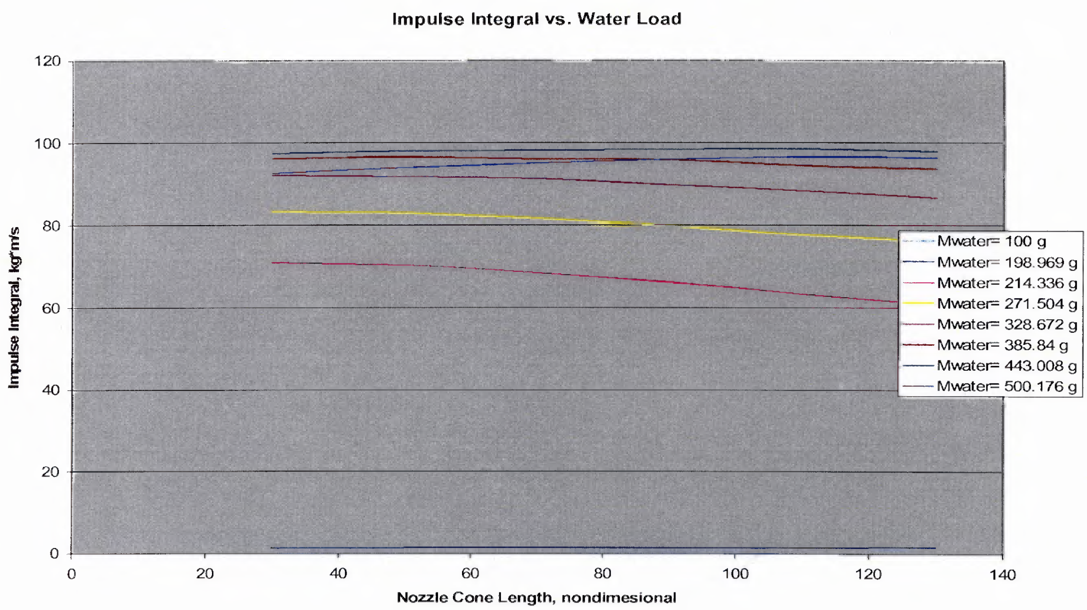

Figure B.20 Impulse integral versus water load distribution plot with L_{bar}=380e-3, D_n2=5e-3, and D_n1=64e-3.

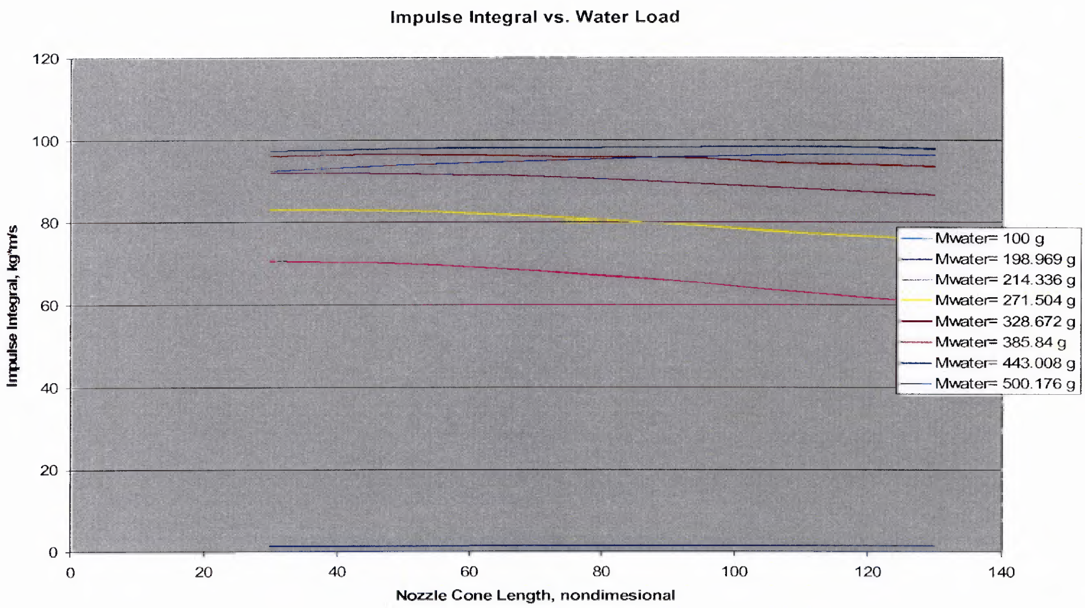

Figure B.21 Impulse integral versus water load distribution plot with L_{bar}=700e-3, D_n2=5e-3, and D_n1=64e-3.

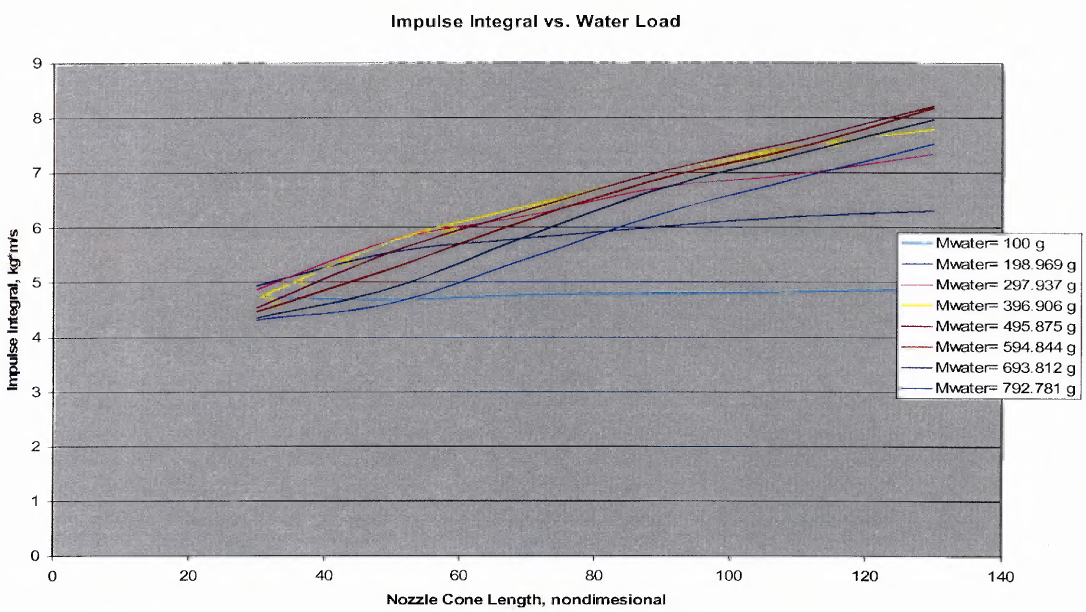

Figure B.22 Impulse integral versus water load distribution plot with L_{bar}=280e-3, D_n2=15e-3, and D_n1=64e-3.

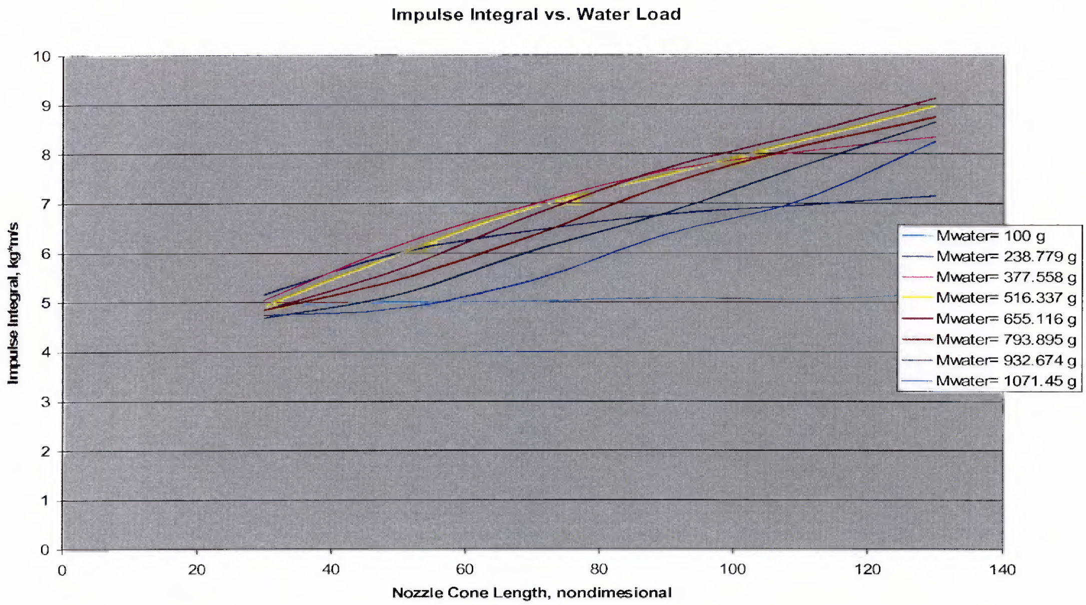

Figure B.23 Impulse integral versus water load distribution plot with L_{bar}=380e-3, D_n2=15e-3, and D_n1=64e-3.

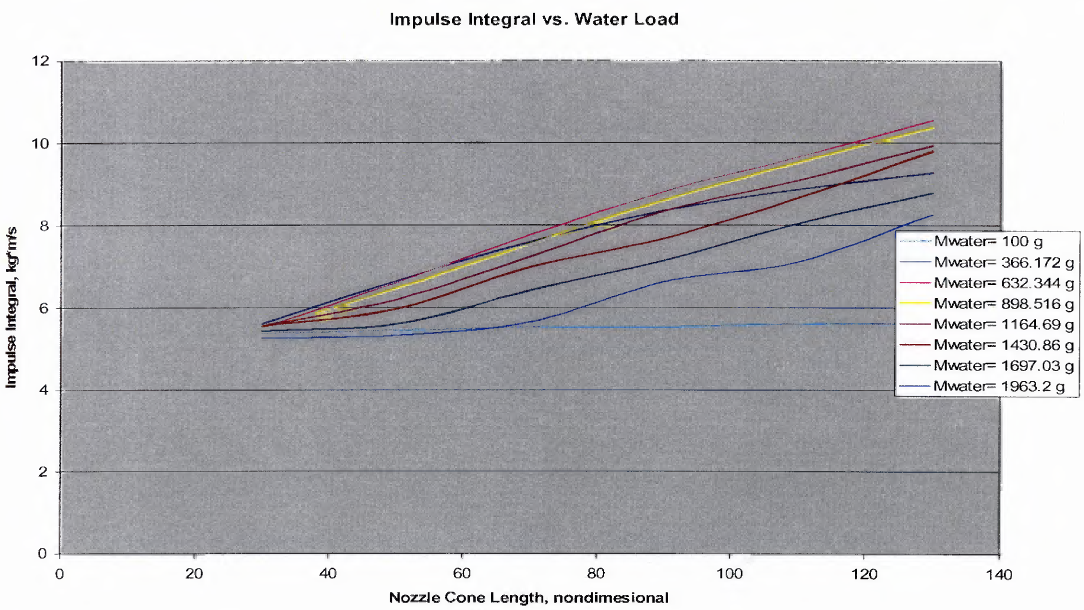

Figure B.24 Impulse integral versus water load distribution plot with L_{bar}=700e-3, D_n2=15e-3, and D_n1=64e-3.

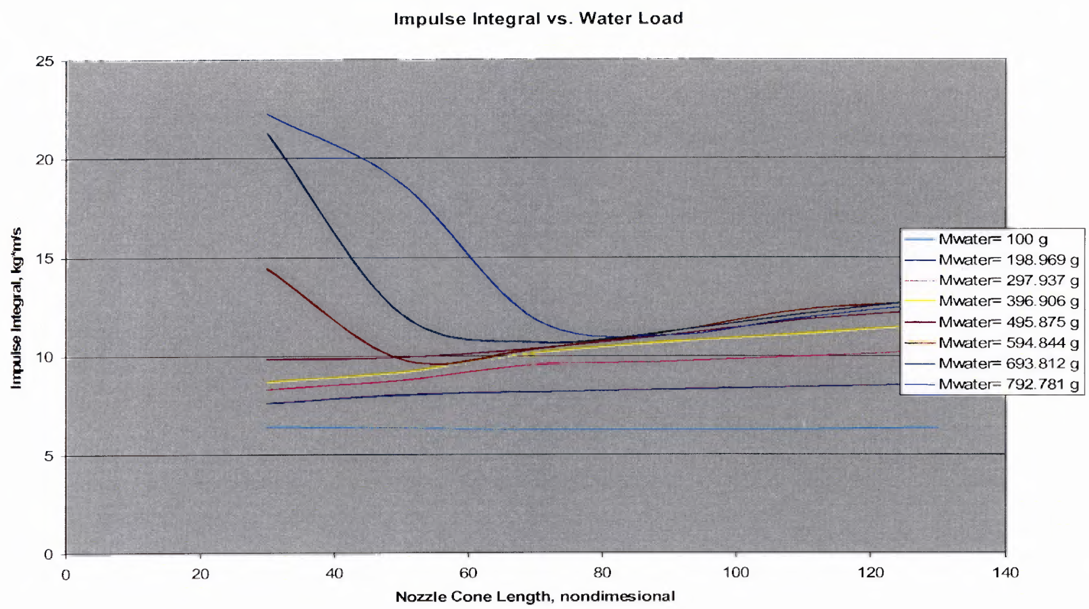

Figure B.25 Impulse integral versus water load distribution plot with L_{bar}=280e-3, D_n2=20e-3, and D_n1=64e-3.

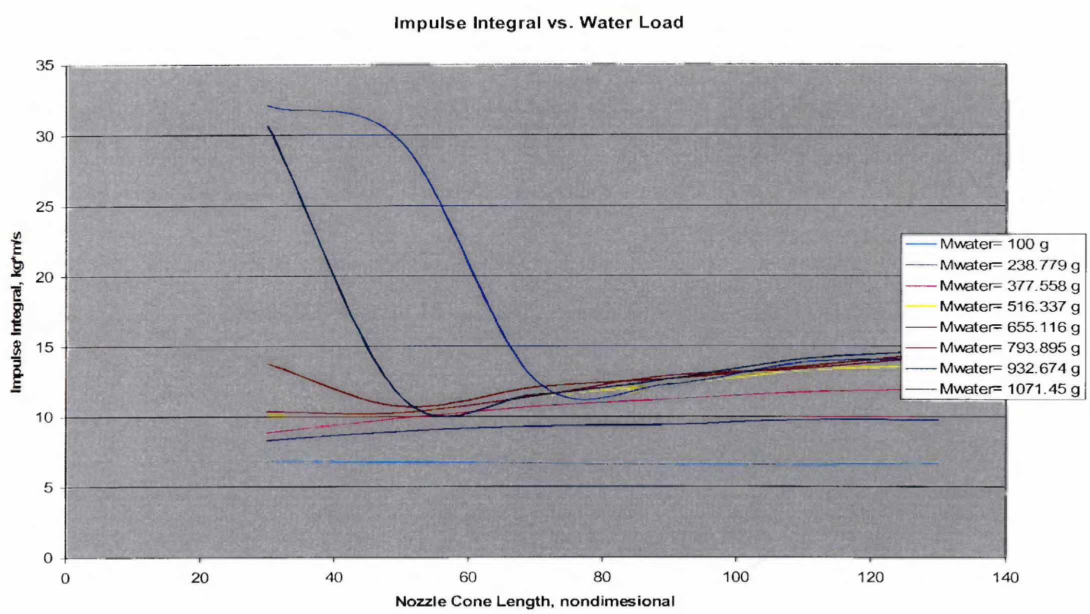

Figure B.26 Impulse integral versus water load distribution plot with L_{bar}=380e-3, D_n2=20e-3, and D_n1=64e-3.

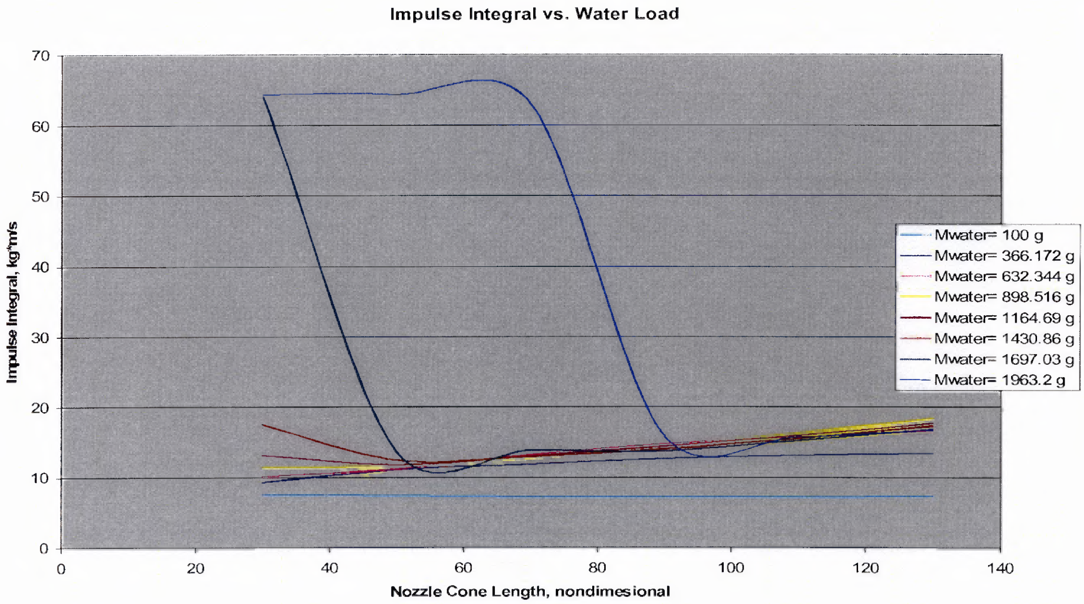

Figure B.27 Impulse integral versus water load distribution plot with L_{bar}=700e-3, D_n2=20e-3, and D_n1=64e-3.

REFERENCES

1. Atanov, G.A. (1977). Internal ballistics of hydro cannon and impulsive water extruder. Donetsk, USSR: Donetsk State University.

2. Godunov, S.K. et al. Numerical solving multidimensional problems of gas dynamics., Moscow, USSR: Nauka.

3. Petrenko O., Geskin E. S., Atanov G. A., Semko A., Goldenberg B. (2004). Numerical modeling of formation of high-speed water slugs. Newark, NJ: NJIT.

4. Petrenko O.P., Bitadze T. G., Geskin E.S. (2005). Application of numerical techniques for optimization of the water cannon design. *2005 WJTA American Waterjet Conference*. (August 21-23). Houston, Texas.

5. Geskin E.S., Petrenko O.P., Samardzic V., Bitadze T. G. (2004). Army demo report. Newark, NJ: NJIT.

6. Atanov, G.A. (1987). Hydro-impulsive installations for rocks breaking. Kiev, USSR: Vystcha shkola.

7. Atanov G. (1996). The impulsive water jet device: A new machine for breaking rock. International Journal of Water Jet Technolgy (Vol. 1, No 2). (pp. 85-91).

8. Atanov, G.A., Semko, A.N. (1987). About correlation between the dynamic ultra jet pressure and the static pressure in the installation. Aerogazodinamika. Tomsk. Tomsk State University (pp. 9-13).